

Chapter 4 High Mobility in Modulation-Doped Si

Two-Dimensional Electron Gases

4.1 Introduction

The two-dimensional electron gas (2DEG) in semiconductors is a fundamental low-dimensional system [63] for condensed matter physics. Important physical phenomena such as the integral and the fractional quantum Hall effects were discovered in high-quality 2DEGs [64, 65]. Furthermore, practical applications such as modulation-doped field-effect transistors (MODFETs) [66] or quantum computation [12] were also realized by utilizing a 2DEG. The most important feature of a 2DEG is its high electron mobility using the so-called modulation-doping technique to separate the supply impurities and electrons [67]. A record high mobility of $3.5 \times 10^7 \text{ cm}^2/\text{V}\cdot\text{s}$ was demonstrated in a GaAs 2DEG at $T < 1 \text{ K}$ [68]. In silicon, the electron confinement could be achieved in the inversion layer of Si MOS structure [64]. However, strong scattering from the impurity charges of the Si/SiO₂ interface has restricted the electron mobility to the level of $2 \times 10^4 \text{ cm}^2/\text{V}\cdot\text{s}$ [69].

In 1985, Abstreiter *et al.* showed that electrons can be confined in a strained Si layer sandwiched between the relaxed SiGe layers [70]. In their Si/SiGe heterostructure, the mobility was fairly low ($\sim 2000 \text{ cm}^2/\text{V}\cdot\text{s}$) due to the high density of dislocation defects by a large lattice mismatch between Si and SiGe layers. With a thick graded Si_{1-x}Ge_x layer ($0 < x < 0.3$) of several microns grown on a Si substrate followed by a

relaxed Si_{0.7}Ge_{0.3} layer, Ismail *et al.* demonstrated a much improved mobility of 535,000 cm²/V-s [71]. A yet higher electron mobility of 800,000 cm²/V-s was reported by Sugii *et al.* with a combination of MBE and solid phase epitaxy to provide an atomically flat interface, reducing the interface roughness scattering [72]. On the other hand, Huang *et al.* recently demonstrated a record high mobility of 2×10^6 cm²/V-s in their enhancement-mode device of undoped Si 2DEG by top gating (no modulation doping), and suggested the background impurity scattering as the limiting factor of electron transport [73].

To summarize, the dominant scattering source in Si 2DEGs appeared very different for various structures and there is no systematic work on the effects of the layer structure on electron transport properties in a Si 2DEG so far. In this chapter, the basic properties of a 2DEG will first be briefly introduced, followed by our experimental results of modulation-doped Si 2DEGs of different layer structures. We also demonstrate effective Schottky gating on a modulation-doped Si 2DEG in order to manipulate the electron density and mobility so as to identify the dominant scattering mechanisms.

4.2 Characteristics of a Si 2DEG

4.2.1 Band Offset between Strained Si and Relaxed SiGe layers

For a strained SiGe layer grown pseudomorphically on a relaxed Si substrate, such as the heterojunction tunneling devices in chapter 2, the entire band offset is almost in the valence band, providing hole confinement [74]. On the other hand, for electron confinement, a tensile strained Si layer must be sandwiched between relaxed SiGe

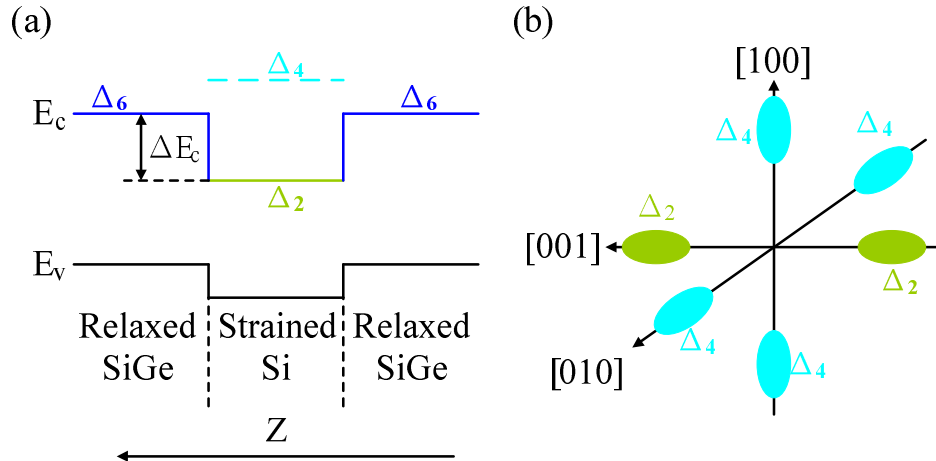


Fig. 4.1 (a) Band diagram of a relaxed-SiGe/strained-Si/relaxed-SiGe heterostructure. The energy levels in the conduction band of strained Si are split into two states: Δ_2 and Δ_4 ; (b) under tensile strain, electrons reside in the two states of Δ_2 along (001) in Si with an in-plane effective mass of $m^* = 0.19 m_0$ [75].

layers (Fig. 4.1 (a)). A conduction band offset (ΔE_c) exists between a strained Si layer and a relaxed SiGe layer because the six degenerate valleys in the conduction band of the strained Si layer split into two sub-sets of Δ_4 and Δ_2 (Fig. 4.1(b)) [75]. Due to the lower energy level of Δ_2 states than that of Δ_4 states, the electrons are in Δ_2 states. In relaxed SiGe layers, the degeneracy of six is preserved. The conduction band offset ΔE_c between a strained Si layer and a relaxed SiGe layer represents the energy difference between the conduction band edge in SiGe and the energy level of Δ_2 in Si, which depends on the Ge fraction in the SiGe layer.

4.2.2 Layer Structure and Epitaxial Growth

A typical layer structure of a Si 2DEG and the associated band energy diagram are shown in Fig. 4.2. From the substrate to the surface, there are several epitaxial layers:

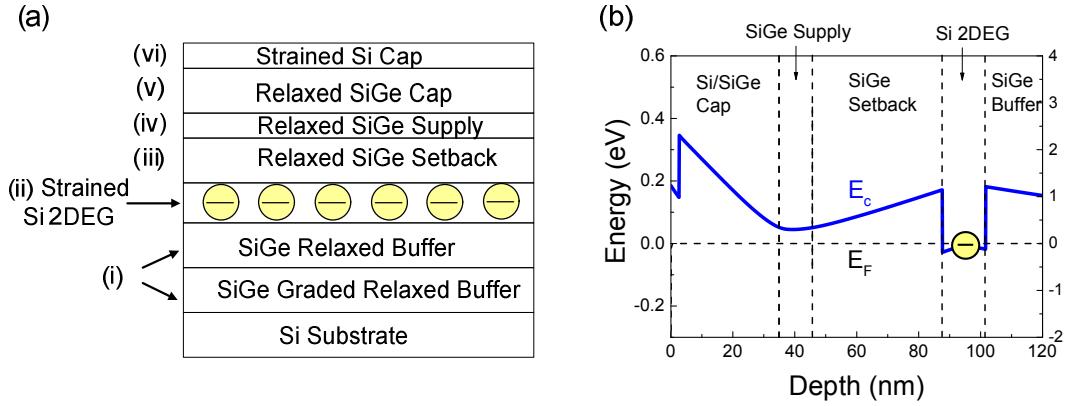


Fig. 4.2 (a) Layer structure of a Si 2DEG and (b) the associated band diagram with a Ge fraction of 0.27 in a Si/SiGe heterostructure without gate bias.

- (i) $\text{Si}_{1-x}\text{Ge}_x$ graded buffer ($0 < x < 0.27$ for this work) + $\text{Si}_{0.73}\text{Ge}_{0.27}$ relaxed buffer,
- (ii) strained Si quantum well (2DEG),
- (iii) relaxed $\text{Si}_{0.73}\text{Ge}_{0.27}$ setback,
- (iv) relaxed $\text{Si}_{0.73}\text{Ge}_{0.27}$ supply of electrons,
- (v) relaxed $\text{Si}_{0.73}\text{Ge}_{0.27}$ cap,
- (vi) strained Si cap.

The basic functions of these layers in a Si 2DEG are described as follows: first, the $\text{Si}_{1-x}\text{Ge}_x$ graded layer ($0 < x < 0.27$) provides a buffer between the growth interface and the Si 2DEG layer on top. Due to the large lattice mismatch between Si and SiGe, the misfit dislocations exist at the growth interface and the threading dislocations punch through the 2DEG layer [19]. With a slow grading rate of 10% Ge/ μm , a misfit dislocation as low as $5 \times 10^5 \text{ cm}^{-2}$ was achieved in a $\text{Si}_{1-x}\text{Ge}_x$ graded buffer ($0 < x < 0.3$) [76]. Next, a thick relaxed SiGe layer of constant Ge fraction is grown on top of the $\text{Si}_{1-x}\text{Ge}_x$ graded layer. This layer offers a buffer between the buried dislocations and the

2DEG layer on top to reduce the electron scattering by those dislocations.

For (ii), a strained Si layer - where the 2DEG resides - is grown between two relaxed $\text{Si}_{0.73}\text{Ge}_{0.27}$ layers, forming a quantum well for electron confinement. The thickness of this layer is limited by the critical thickness of a strained Si layer on a relaxed SiGe layer, so as to prevent any further induced dislocations. A relaxed $\text{Si}_{0.73}\text{Ge}_{0.27}$ setback layer (iii) not only provides the required energy confinement for electrons in the Si QW layer, but also separates the supply layer of ionized impurities from the 2DEG, leading to less impurity scattering. With the remote supply layer of n-type doping (iv), electrons can be “supplied” to the Si QW layer. Due to the separation of 2DEG and those ionized impurities in the supply layer, electron scattering can be significantly reduced, resulting in very high electron mobility.

Due to the surface segregation of the n-type dopants in the SiGe layers (chapter 3), a thick SiGe cap layer (v) has to be grown to avoid a high doping level at the surface which induces high gate leakage current through a Schottky barrier on the surface. Finally, a Si cap layer offers a much more stable surface than a SiGe layer, which is crucial for the subsequent processing steps.

In our work, the relaxed SiGe buffer layers were provided by Amberwave Inc. with a graded $\text{Si}_{1-x}\text{Ge}_x$ layer ($0 < x < 0.27$) of a grading rate of 10% Ge/ μm grown on top of Si substrates followed by a $\text{Si}_{0.73}\text{Ge}_{0.27}$ buffer layer of 2 μm . Chemical mechanical polishing (CMP) was applied to reduce the surface roughness prior to the epitaxial growth. The wafers were cleaned by the following steps: 5 min in diluted HF (1%), 15 min in H_2SO_4 : H_2O_2 (2.5:1), followed by 2 min in diluted HF (1%). Next, the wafers were heated to 850 °C for 5 min in hydrogen gas at 6 torr to remove the residual oxide

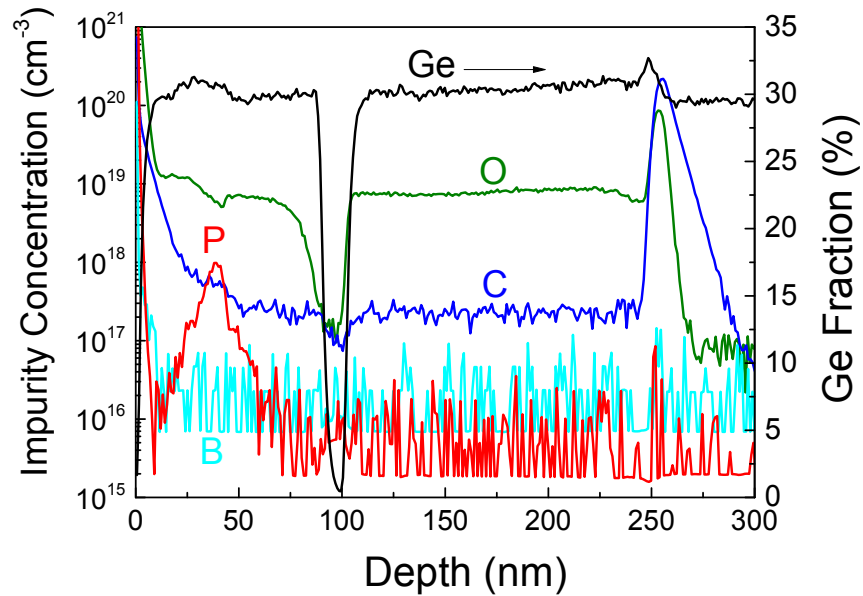


Fig. 4.3 SIMS analysis of a typical Si 2DEG (sample #5737). Ge, P, B, C, and O were measured from the surface to below the growth interface at a depth of 255 nm.

before the epitaxial growth began. The flow rate of hydrogen was 3 slm. Diluted SiH_4 (10 % in argone) of 50 sccm and GeH_4 (0.8 % in hydrogen) of 76 sccm were used for the growth of the Si and SiGe epitaxial layers. The growth rates of Si at 625 °C and SiGe at 575 °C were 0.5 nm/min and 5 nm/min, respectively. Diluted phosphine (100 ppm in hydrogen) of 2 sccm was used as a doping gas for the growth of an n-type SiGe supply layer. After baking, a SiGe buffer layer of 100 ~ 150 nm was grown at 575 °C, followed by a strained-Si layer (2DEG layer) of 6 ~ 30 nm at 625 °C, a SiGe setback layer of 10 ~ 70 nm at 575 °C, a n-type SiGe supply layer of 10 nm at 575 °C with a doping level between 10^{18} to 10^{19} cm^{-3} , a SiGe cap layer of 20 ~ 50 nm at 575 °C, and a Si cap layer of 2 nm at 625 °C.

The layer thicknesses, doping level and Ge fraction were measured by SIMS.

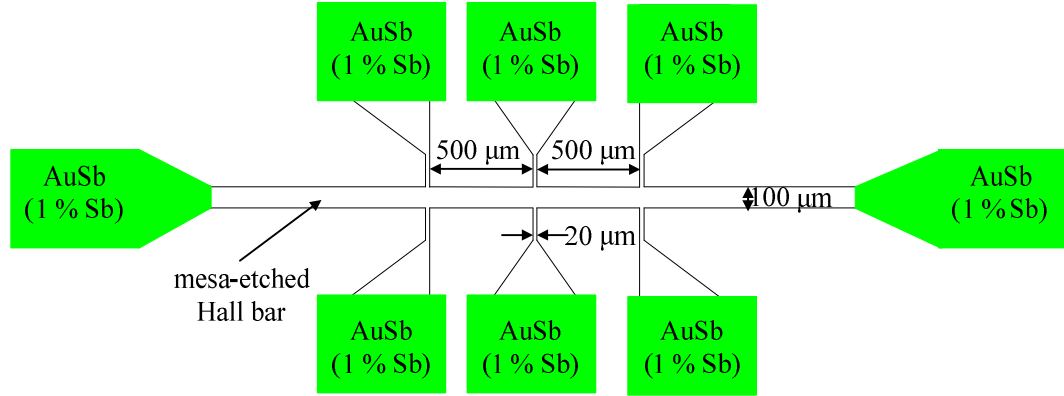


Fig. 4.4 Top view of a typical Hall bar device. Hall bar was first mesa-etched by RIE followed by alloyed AuSb (1 % Sb) for electrical contacts.

Ge, P, B, C, and O in a typical modulation-doped Si 2DEG (sample # 5737) are plotted versus depth in Fig. 4.3. At a depth of 96 nm, a strained Si QW layer of 12 nm is sandwiched between the relaxed SiGe layers. The thickness of the SiGe setback layer is 50 nm between the upper SiGe/Si interface and the position of the peak phosphorus level. The surface segregation of phosphorus was suppressed with a turn-off slope of 13 nm/decade in the SiGe cap layer, which was grown at 525 °C. At the re-growth interface of depth 255 nm, a spike of C and O indicates the incomplete removal of contaminants. Although baking at higher temperatures can be used for the better cleaning of the growth interface, dislocations can be created via the strain relaxation of the underlying graded $\text{Si}_{1-x}\text{Ge}_x$ layer. Thus, other approaches such as in-situ cleaning using HCl or HF [77], or a thick SiGe buffer layer which increases the distance of remote scattering at the growth interface to 2DEG [78], were suggested. In this work, the latter approach was used and the experimental results are presented in section 4.4.1. The C levels in the SiGe and Si layers are 1.8×10^{17} and $8 \times 10^{16} \text{ cm}^{-3}$, respectively. The O levels in the SiGe and Si layers are 7.3×10^{18} , and $1.5 \times 10^{17} \text{ cm}^{-3}$, respectively.

After the growth, the wafers were mesa-etched to the Hall bar geometry, followed by AuSb deposition (1% Sb) and annealing at 450 °C over 10 minutes for electrical contacts. For the gating experiment (in section 4.5), palladium was thermally evaporated in order to cover the entire Hall bar for Schottky gating on single 2DEG devices. The typical Hall bar device is shown in Fig. 4.4. For low-temperature measurements, samples were first wire bonded and dipped into a liquid helium dewar at 4 K or 0.3 K. The Hall measurements were performed by lock-in technique to measure the longitudinal (R_{xx}) and transverse (R_{xy}) magneto-resistances for the analysis of electron density and mobility. The typical drive current is 100 nA.

4.2.3 Electrostatics

In this section, we focus on the electrostatics of a Si 2DEG. With a simulator solving Poisson's and Schrödinger's equations at the same time [23], the energy diagram of the conduction band in a Si 2DEG at 4 K is plotted in Fig. 4.5. Two boundary conditions were assumed for this band diagram. First, the Fermi level (E_F) is pinned at the midgap of the Si surface layer due to the presence of many surface defects. The second boundary condition is that E_F is also pinned at the donor level (E_d) in the supply layer, since the devices were measured at low temperatures. The electron density of the 2DEG can be solved by the following equation [79]:

$$\Delta E_C = E_{edge} + E_d + \frac{e^2 N_d L^2}{2\epsilon\epsilon_0} + \frac{e^2 n_{2D} d}{\epsilon\epsilon_0}, \quad (4.1)$$

where E_d is the energy difference between the donor level and the conduction band edge in the SiGe layer, E_{edge} is the energy difference between E_F and the conduction band

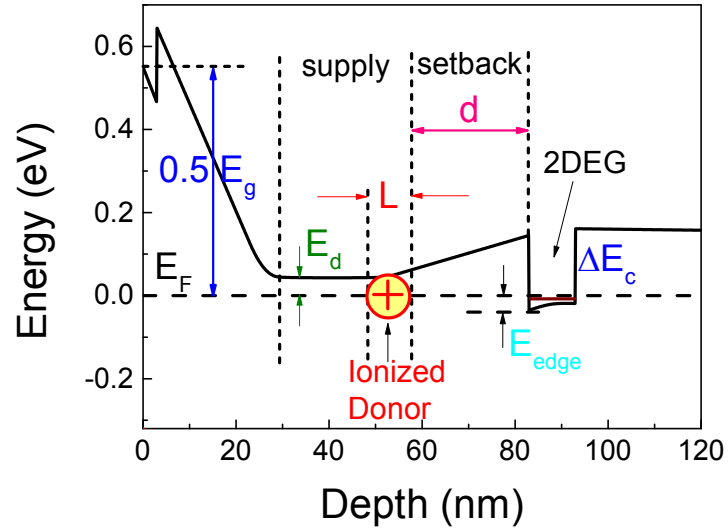


Fig. 4.5 Conduction band diagram of a Si 2DEG at 4 K with two boundary conditions for the Fermi level (E_F) to be pinned at (i) the mid-gap of Si surface and (ii) the donor level.

edge at the upper SiGe/Si interface, and the last two terms represent the energy drop across the ionized impurity in the charged supply layer of length L and the neutral setback layer of length d . We assume zero doping in the Si QW and in the structure below the QW, so the electric field below the quantum well is zero.

Since the typical 2DEG density and the doping level are on the order of 10^{11} cm^{-2} and 10^{18} cm^{-3} , respectively, the required width L can be calculated by $N_d L = n_{2D} \sim 1 \text{ nm}$, which is much smaller than the thickness of the setback layer ($20 \sim 70 \text{ nm}$). Therefore, the third term in Eq. (4.1) is usually ignored. Furthermore, because E_{edge} of \sim hundreds μeV is fairly small compared to ΔE_c ($\sim 180 \text{ meV}$ for $\text{Si}_{0.7}\text{Ge}_{0.3}$ [80]), to first order only, the second and last terms are considered in the analysis. The electron density n_{2D} in the Si QW layer can be solved as:

$$n_{2D} \approx \frac{\epsilon\epsilon_0}{e^2} \frac{\Delta E_C - E_d}{d}. \quad (4.2)$$

This shows that the density at equilibrium (without external gating) can be manipulated by adjusting the conduction band offset (i.e., changing the Ge fraction in the SiGe barrier) or the thickness of the setback SiGe layer. In this work, the Ge fraction is fixed at 0.27 and we focus on the effect of the SiGe setback layer thickness on 2DEG characteristics (section 4.4.3).

4.2.4 Mobility Model

To investigate the scattering mechanisms in a Si 2DEG, we followed the procedures derived by Davies [79]. For quantum dot applications, achieving a single electron would require a low density in a 2DEG or a small dot area by a simple relation of $1 = n_{2D} \times \text{Area}$. With a QD of 30 nm \times 30 nm (typical of advanced lithography), n_{2D} must be at most $\sim 1 \times 10^{11}$ cm⁻². Thus, we focus on the transport properties of the 2DEGs at densities below 4×10^{11} cm⁻², where remote or background impurity scattering has been suggested as the dominant scattering mechanism [81, 82].

The strongest scattering at low temperatures in many 2DEG systems arises from ionized impurities such as n-type donors in the supply layer or throughout the entire material. The former is usually called ‘remote impurity scattering’ and the latter is usually referred to as ‘background impurity scattering’ [79, 82]. For remote impurity scattering, we assumed for simplicity that the supply layer is delta-doped with a two-dimensional density of N_{imp} ionized impurity, and located at a distance of d from the doping plane to the edge of the Si QW layer. The resulting electron transport time based

on Fermi-Golden's rule can be expressed as [79]

$$\frac{1}{\tau_{tr}} = \frac{\hbar N_{imp}}{32m^* d^3 \sqrt{\pi n_{2D}^3}}, \quad (4.3)$$

where m^* is the effective mass of electron in the Si QW layer and the effects of the degeneracy of the two valley states and two spin states were already included. Next, the mobility ($\mu = \frac{e\tau_{tr}}{m}$) is given by

$$\mu_{remote} = \frac{32ed^3 \sqrt{\pi n_{2D}^3}}{\hbar N_{imp}}. \quad (4.4)$$

When n_{2D} increases, there is stronger electron screening [79] and so the mobility increases. As the distance between the plane of ionized impurities and the 2DEG increases, electron scattering is weaker and the mobility is higher. On the other hand, as the number of ionized impurities is reduced, the remote scattering becomes weaker and the mobility increases.

Ideally, in a 2DEG structure, the only doped region is the supply layer. However, in practice - in other layers a minimum level of certain types of impurities exists, depending upon the reactor history and growth conditions. The ionized background impurities across the entire sample also scatter the 2DEG with a predicted mobility as:

$$\mu_{background} = \frac{2e\sqrt{n_{2D}}}{\sqrt{\pi}\hbar N_{background}}. \quad (4.5)$$

In a similar manner to remote impurity scattering, as the electron density increases, the background impurity scattering is reduced due to stronger electron screening. When the

number of ionized background impurities is reduced, the scattering will be weaker.

The total mobility related to these two types of impurities can be written as:

$$\frac{1}{\mu_{total}} = \frac{1}{\mu_{remote}} + \frac{1}{\mu_{background}}. \quad (4.6)$$

In the next section, we will show the importance of background scattering in a Si 2DEG that has been grown. Afterwards, we present a much improved mobility by reducing the background impurity level in the CVD system at Princeton University.

The above model of 2DEG mobility was proposed with several assumptions, such as the delta doping in the supply layer. In practice, broadened n-type doping profiles in the SiGe layer are caused by strong surface segregation (chapter 3), which might offset the predicted mobility by the above model. Furthermore, the abruptness of the SiGe/Si/SiGe heterostructure may not be perfectly sharp, resulting in a perturbation on the quantum states in the Si QW layer. During the derivation for electron screening, many numerical approximations were made [79]. This made the derivation easier, but is not of spectacular accuracy. As a result, in this work, we use this theoretical model only as a rough guide to help us to understand the electron transport properties, but not for any precise numerical fitting or model comparison with our data.

4.3 Efforts Toward High Mobility in Si 2DEGs

4.3.1 Effects of Phosphorus Background Impurity on 2DEG Mobility

In CVD systems, the background level of n-type dopants such as phosphorus or arsenic may be very high due to the memory effect [83]. In Fig. 4.6, the SIMS data of a typical Si 2DEG (sample # 5144) is illustrated. The gas precursors for the epitaxial

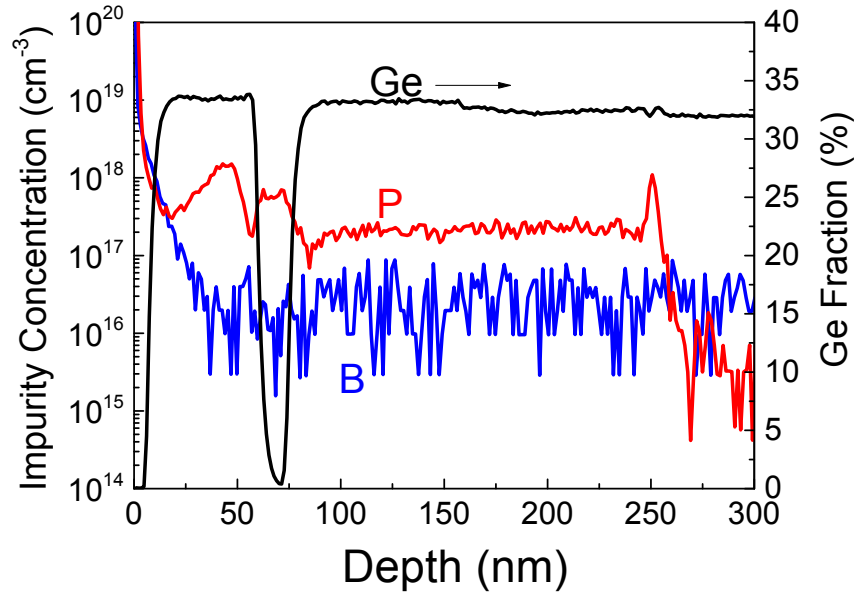


Fig. 4.6 SIMS results of a Si 2DEG (sample #5144). The phosphorus background levels in the Si and SiGe layers are $6 \times 10^{17} \text{ cm}^{-3}$ and $2 \times 10^{17} \text{ cm}^{-3}$, respectively.

growth of this sample were SiH_2Cl_2 and diluted GeH_4 with diluted PH_3 as the n-type doping gas. At a depth of 40 nm, a phosphorus doped layer of $1.5 \times 10^{18} \text{ cm}^{-3}$ was grown. The phosphorus background levels in the Si and SiGe layers are $6 \times 10^{17} \text{ cm}^{-3}$ and $2 \times 10^{17} \text{ cm}^{-3}$, respectively. Note that below the growth interface at 250 nm, the phosphorus level in the relaxed buffer grown by Amberwave Inc. is below 10^{15} cm^{-3} , showing that the phosphorus levels in the epitaxial layers grown by our CVD are true and not artifacts or detection limits from the SIMS measurements. By assuming $n_{2D} \sim 5 \times 10^{11} \text{ cm}^{-2}$ and ignoring the remote impurity scattering, the electron mobility at a background impurity of $5 \times 10^{17} \text{ cm}^{-3}$ can be estimated by Eq. (4.5) as $5,000 \text{ cm}^2/\text{V-s}$, which is close to our experimental results of $3,000 \sim 8,000 \text{ cm}^2/\text{V-s}$. Thus, the first task in improving the 2DEG mobility is to lower the background impurity level in the epitaxial layers.

4.3.2 The Reduction of Phosphorus Background Impurity Levels

A low phosphorus background level has been suggested for a 2DEG of high mobility. In this section, we will introduce the means by which we identified the sources for high background level of phosphorus in our CVD system, followed by an approach to reduce the phosphorus level and our experimental results.

First, we evaluate the impact of the potential sources for a high phosphorus level, such as the quartz tube and the quartz wafer holder. Since the Si wafers were often baked or annealed at high temperatures (~ 1000 °C) in our CVD system, phosphorus adsorbed on the quartz walls might desorb and incorporate into the epitaxial films. To remove the coated phosphorus on the quartz wall and the wafer stand, we used HF:HNO₃:H₂O (1:4: 6) to etch the deposited films on the quartz surface, followed by a DI water rinse. However, in a test 2DEG structure grown after the wet cleaning steps, the phosphorus background level was rather high ($\sim 10^{17}$ cm⁻³) and the mobility was still low (5,000 \sim 10,000 cm²/V-s). Even with a brand new tube and wafer stand used for the growth of 2DEG devices, identical results of the high background level of phosphorus and low mobility were obtained. This suggests that the main source of phosphorus contamination was not the tubes or wafer stands.

In addition to the quartz tube and stand, the manifold for gas mixing in the gas supply system could be another source of phosphorus contamination. To overcome this problem, we designed a gas delivery system which isolates PH₃ and other gases (Fig. 4.7). The distance from the mixing valve of PH₃ and other process gases to the chamber is 90 cm. The phosphorus level is expected to be lower than that in the old panel

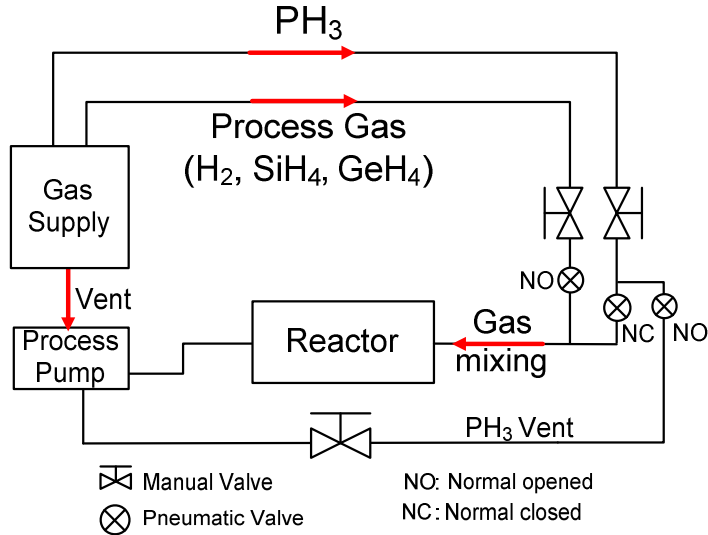


Fig. 4.7 New gas supply system with separation of process gases (H₂, SiH₄, GeH₄, etc.) from PH₃ to reduce the memory effect of phosphorus.

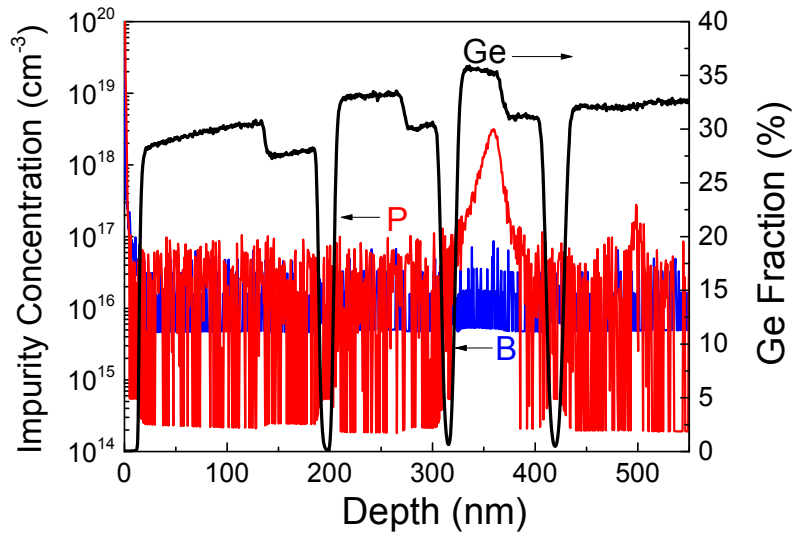


Fig. 4.8 B, P, Ge profiles of a test structure of multiple Si and SiGe layers grown. Both the B and P levels are down to the SIMS detection limits of 5×10^{15} and 3×10^{14} cm⁻³, respectively, except for a phosphorus doped layer grown at the depth of 360 nm.

because there is only a small proportion of tubing which could have a memory effect to contaminate the other process gases. The SIMS results of a test structure of an undoped 2DEG structure (sample #5503) grown by this new gas panel supported our concept (Fig.

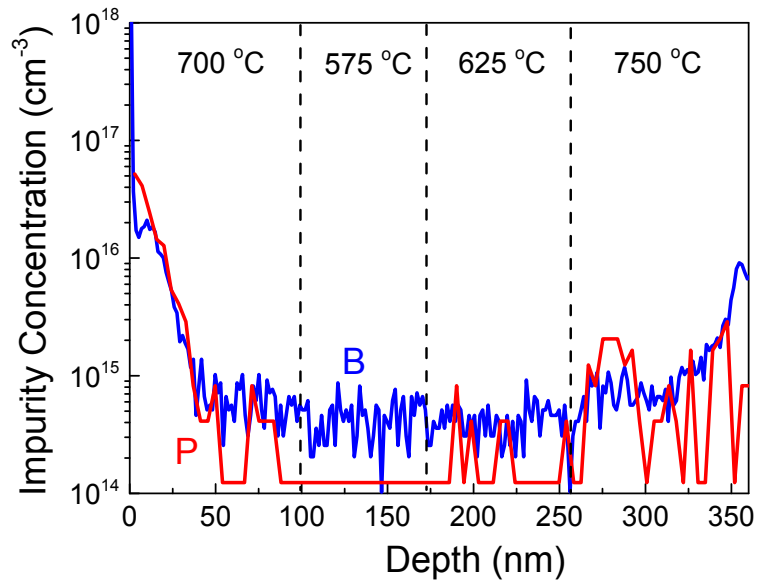


Fig. 4.9 P and B profiles in Si layers grown at different temperatures (sample #5823).

4.8). The boron level and the phosphorus level are as low as the SIMS detection limits of $5 \times 10^{15} \text{ cm}^{-3}$ and below 10^{15} cm^{-3} , respectively. In this sample, a phosphorus doped layer was grown at the depth of 360 nm. The phosphorus levels before PH_3 turn-on and after PH_3 turn-off are identical, showing that the memory effect is insignificant using the new gas panel equipped with the gas separation system.

A test sample was grown after more than 100 runs of 10 μm deposition in the reactor to confirm the negligible memory effect of phosphorus in the entire system. In this sample, only Si layers were grown at different temperatures, with very thin SiGe layers as indicators for the SIMS analysis (Fig. 4.9). For phosphorus, in the Si layer grown below 750 °C, its level is as low as the detection limit of $1.5 \times 10^{14} \text{ cm}^{-2}$, which is three orders of magnitude lower than the level by using the old gas panel. Between 260 to 350 nm, the phosphorus level is slightly higher. Probably because the layer was

grown immediately after high temperature baking, the desorption of the absorbed phosphorus on the quartz wall was stronger, leading to higher incorporation into the films. For boron, although it is as low as $3 \times 10^{14} \text{ cm}^{-3}$, it is surprising that its level is slightly higher, since a boron precursor has never been used in the new gas panel. The low boron level in the system could be a SIMS effect or the auto-doping from the lightly boron-doped SiGe relaxed buffer substrates grown by Amberwave Inc.

4.3.3 Transport Properties of Si 2DEGs with Low Phosphorus Background Impurity Levels

To estimate the effect of a low background level of mid 10^{14} cm^{-3} on 2DEG mobility, we assumed that the 2DEG mobility is limited by the background impurity scattering. Using Eq. (4.5), we estimated a mobility of $3 \times 10^6 \text{ cm}^2/\text{V-s}$, which is almost 10 times higher than the highest mobility reported in this work. Therefore, it is suggested that the mobility in 2DEGs grown by this new gas system is not limited by background impurity scattering, but rather that it is limited by remote impurity scattering. Further experimental results in the following sections confirm our conclusions.

Si 2DEGs of low background impurity were epitaxially grown with the new gas panel and fabricated into Hall bar devices. The low-temperature (4 K and 0.3 K) electron density and mobility of Si 2DEGs with different layer structures (i.e. varying the SiGe setback layer thickness, the doping level, SiGe cap layer thickness, etc.) were measured (Fig. 4.10). The highest mobility was $522,000 \text{ cm}^2/\text{V-s}$ [84], which was ~ 100

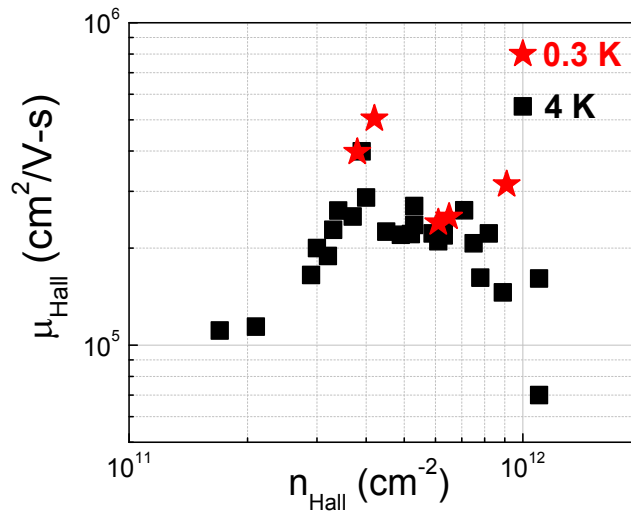


Fig. 4.10 Hall mobility vs. electron density at low temperatures (4 K or 0.3 K). A highest mobility of 522,000 cm²/V-s was measured at 0.3 K [84]. Note that each data point was taken from different samples with different layer structures.

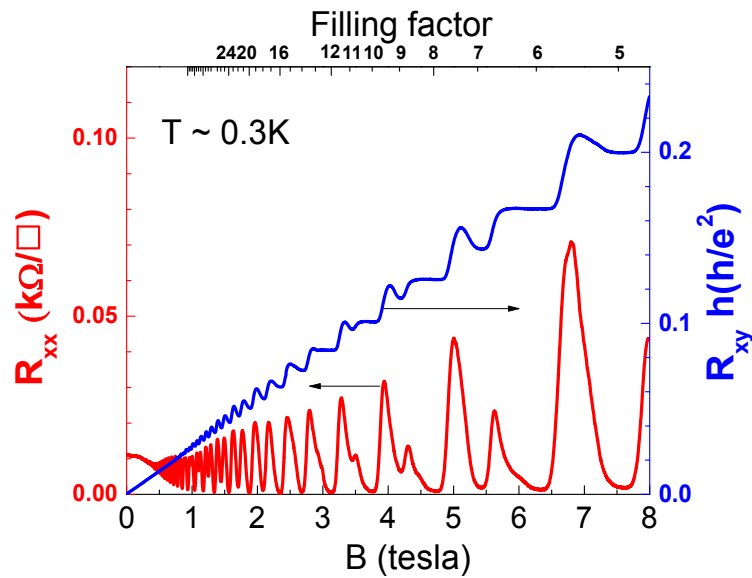


Fig. 4.11 Longitudinal (R_{xx}) and transverse (R_{xy}) magneto-resistances vs. magnetic field at 0.3 K [84].

times higher than the level of the samples grown by the old gas panel. The longitudinal (R_{xx}) and transverse (R_{xy}) magneto-resistances of sample #5446 were also measured at

0.3 K by Prof. Rokhinson at Purdue University (Fig. 4.11). Clear Shubnikov-de Haas oscillations in R_{xx} and quantum Hall plateaus in R_{xy} were observed, showing the high quality of this sample. The spin splitting and valley splitting occurred at 0.8 T and 3.5 T, respectively. Overshoots of R_{xy} at odd filling factors were observed. Several suggestions have been made to explain such effects, such as a rapid decoupling of overlapping spin-split states [85] and a mixing of overlapping edge states and the intrinsic spin-orbit interaction of 2DEGs [86]. These effects are beyond the scope of this thesis.

4.4 Effects of Layer Structure on 2DEG Mobility

4.4.1 SiGe Buffer Layer

Typically, a Si 2DEG structure is epitaxially grown on a Si (100) substrate, either by MBE or CVD. In Princeton, we grew the epitaxial layers of a Si 2DEG on a virtual substrate which consisted of a relaxed SiGe buffer layer on top of a graded SiGe layer on a Si substrate (provided by Amberwave Inc.). Prior to the growth, chemical mechanical polish was applied to reduce the surface roughness, followed by a wet cleaning to remove the residual contaminants and native oxide on the polished relaxed SiGe surface. Next, SiGe and Si epitaxial layers were grown using the new gas supply system, and Hall bar devices were fabricated for electron transport measurement at low temperatures.

As depicted in Fig. 4.3, there were spikes of C and O at the substrate interface due to inefficient cleaning before epitaxy. Paul *et al.* have suggested that with a thick SiGe buffer layer on the SiGe virtual substrate, electron scattering from the bottom

growth interface was much reduced [78]. Therefore, we grew test samples (#5858, #5838, and #5862) with three different thicknesses of the SiGe buffer layer (50, 155, and 310 nm), while the rest of the layer structures in those three samples were identical to each other (Table 4.1).

Table 4.1 Layer structures of sample #5858, #5838, and #5862 for study of the effects of SiGe buffer layer thickness on the 2DEG mobility

Sample #	Growth Temp	Thickness (nm)		
	(°C)	5858	5838	5862
Si cap	625	4	4	4
SiGe cap	550	50 ~ 70	50 ~ 70	50 ~ 70
SiGe supply	575	10	10	10
P level (cm ⁻³)	575	$1 \sim 4 \times 10^{18}$	$1 \sim 4 \times 10^{18}$	$1 \sim 4 \times 10^{18}$
SiGe setback	575	30	30	30
Si QW	625	10	10	10
SiGe buffer	575	50	155	310

The electron mobility measured at a 4 K vs. SiGe buffer layer thickness is shown in Fig. 4.12. The electron mobility was only slightly reduced for the device with the 75-nm SiGe buffer layer, which followed the experimental results in [78]. Although the density of C and O are high, the degree to which they affect the electron transport (e.g., the ionization ratio and charge type) is not yet known. Since the SiGe buffer layer separates the growth interface and the 2DEG, the remote impurity scattering at this interface could be much reduced with a thicker SiGe buffer layer. With 2DEG mobility saturated as the SiGe buffer layer thickness > 150 nm, we think that 2DEG transport is not limited by the remote impurity scattering from the growth interface, and that the mobility does not depend on the levels of C and O at the growth interface.

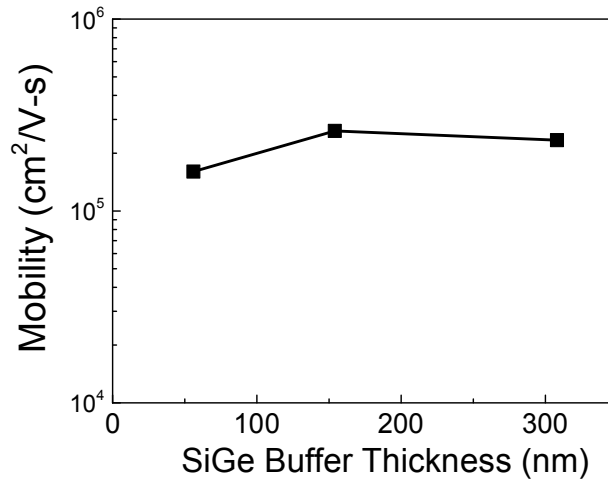


Fig. 4.12 Electron Mobility at 4 K vs. SiGe buffer layer thickness.

4.4.2 Si Quantum Well Layer

Since the 2DEG is in a strained Si layer, several devices with different thicknesses of Si layer grown at 575 °C and 625 °C were made in order to investigate the effects of strained relaxation on 2DEG mobility (Table 4.2). Electron mobility vs. Si

Table 4.2 Layer structures of test samples for study of the effects of Si QW layer thickness on the 2DEG mobility

	Growth Temp (°C)	Thickness	Growth Temp (°C)	Thickness
Si cap	625	4	625	4
SiGe cap	550	50 ~ 70	550	50 ~ 70
SiGe supply	575	10	575	10
P level (cm ⁻³)	1 ~ 4 × 10 ¹⁸		1 ~ 4 × 10 ¹⁸	
SiGe setback	575	30	575	30
Si QW	575	12, 21, 30	625	6, 10, 12, 18, 26
SiGe buffer	575	150	575	150

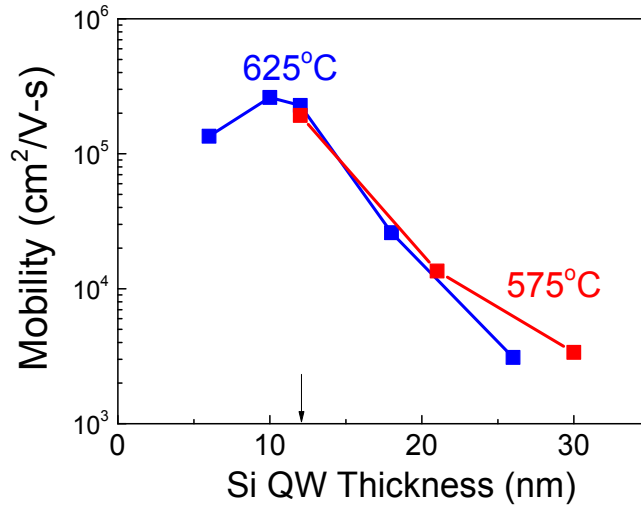


Fig. 4.13 Mobility at a 4 K vs. Si QW layer thickness grown at 575 °C and 625 °C. The arrow indicates the predicted critical thickness of strained Si on the relaxed Si_{0.73}Ge_{0.27} [87].

QW thickness is shown in Fig. 4.13. A peak near 10 nm is observed. For the 625 °C data, the Si QW is thicker than 12 nm, and the mobility drops significantly as the thickness increases. This may be due to dislocations created by the strain relaxation of the thick Si QW layer. The thickness at which mobility drops significantly is close to the reported critical thickness (~ 12 nm) of a strained Si layer on a relaxed Si_{0.73}Ge_{0.27} layer [87]. For 575 °C, a similar trend was observed.

On the other hand, when the Si QW is under 10 nm (e.g. 6 nm), the 2DEG mobility drops slightly when the well is thinner, which could be attributed to the stronger scattering from the roughness at the upper SiGe/Si heterointerface [88]. In a narrow QW, the spreading of electron wavefunction into the SiGe barrier layers becomes stronger, which might also lead to stronger scattering from the remote impurity in the supply layer or alloy scattering in the SiGe barrier [82]. Thus, when we discuss

the ionized impurity scattering in the next section, the thickness of the strained Si QW layer is controlled between 9 to 12 nm and to more easily isolate the effects of different scattering mechanisms on 2DEG mobility.

4.4.3 SiGe Setback Layer

According to the analysis of electrostatics in section 4.2.3, the electron density in the 2DEG layer depends upon the thickness of the SiGe setback layer wherever enough carriers are provided from the supply layer. By adjusting the thickness of the SiGe setback layer, the density can be modulated following Eq. (4.2). The experimental results of electron density vs. the SiGe setback layer thickness is shown in Fig. 4.14(a) with a theoretical calculation of Eq. (4.2). The growth parameters for those devices are listed in Table 4.3. For quantum dot applications, a low electron density is preferred and so a thick setback layer is required. However, for a Si 2DEG of a thick setback layer, the control of patterned top metal gates over the underlying 2DEG will be weaker. Thus, an optimized thickness of a SiGe setback layer is usually used for quantum dot fabrication.

Table 4.3 Layer structures of test samples for study of the effects of SiGe setback layer thickness on the 2DEG mobility.

Layer	Growth Temp (°C)	Thickness (nm)
Si cap	625	4
SiGe cap	550	40 ~ 70
SiGe supply	575	10
P doping level (cm ⁻³)	1 ~ 4 × 10 ¹⁸ cm ⁻³	
SiGe setback	575	12, 20, 30, 40, 50, 70
Si QW	625	10
SiGe buffer	575	150

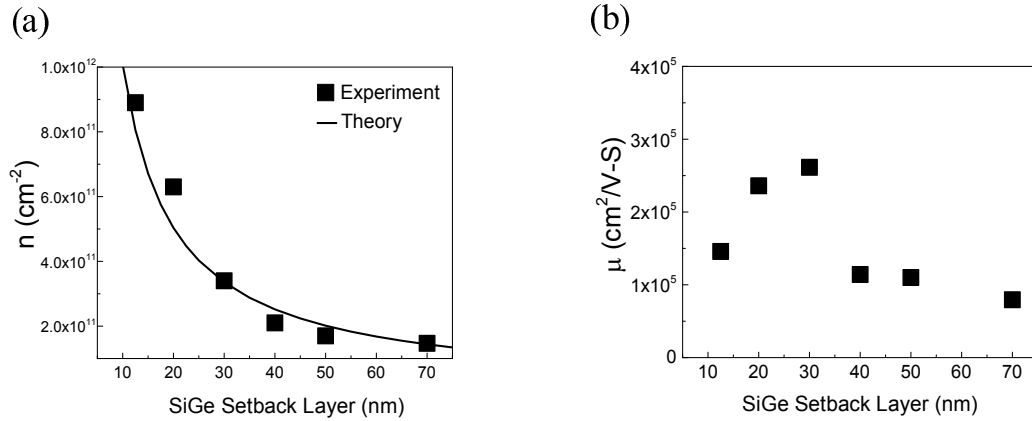


Fig. 4.14 (a) Electron density and (b) mobility vs. SiGe setback layer thickness at 4 K.

In Fig. 4.14(b), electron mobility is also plotted versus the setback layer thickness with a peak mobility at 30 nm. This could be explained as follows: as the setback layer is thicker, the remote impurity scattering from the supply layer becomes weaker – thus, initially the mobility increases. When the thickness of the setback layer is further increased, the electron screening becomes weaker due to lower electron density in the Si QW layer. As such, mobility drops even though the remote scattering itself is reduced with a longer setback distance.

4.5 Extremely Low Electron Density by Effective Schottky Gating in Single 2DEG Devices

In the previous sections, the effects of different layers on 2DEG characteristics were investigated by comparing different 2DEG samples. It is well known that the scattering mechanisms in a 2DEG can be identified and interpreted more accurately in a single device by gating [63]. This allows mobility vs. density to be studied. For a modulation-doped Si 2DEG device, the surface segregation of n-type

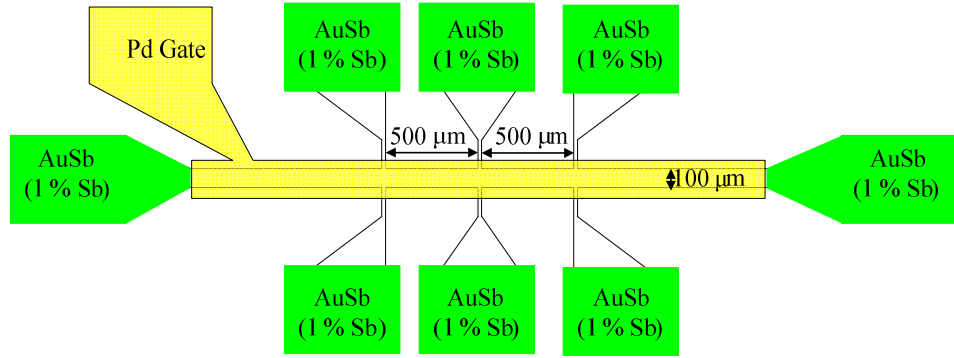


Fig. 4.15 Top view of the Hall bar devices. The contacts were made by AuSb alloying (1 % Sb) and top Pd Schottky gate covers the Hall bar.

dopants leads to a high surface phosphorus level and high gate leakage current. By low-temperature epitaxy [56], we could suppress the segregation significantly (see chapter 3), and effective gating without leakage was enabled [84]. In this section, we present 2DEG characteristics at different densities in a single device obtained by palladium Schottky barrier gating.

Two wafers (#5414 and # 5613) were grown for the leakage test of top Pd Schottky gates covering the entire the Hall bar (Fig. 4.15). P and Ge profiles of these two wafers are illustrated in Fig. 4.16. The layer structures and growth parameters of these two samples are listed in Table 4.4. The growth temperature of the SiGe cap layer for #5414 and #5613 are 575 and 525 °C, respectively. The resulting P turn-off slopes of #5414 and #5613 are 70 nm/dec and 13 nm/dec, respectively. Hall bar devices were fabricated and the leakage current via the Pd Schottky gate were measured at 4 K (Fig. 4.17). For #5414 with a slow P turn-off of 70 nm/dec, the P surface level is above 10^{18} cm^{-3} , leading to a very leaky Hall bar device through the top gate. At low growth temperature of SiGe cap layer (525 °C) for #5613, a P turn-off slope of 13 nm/dec was

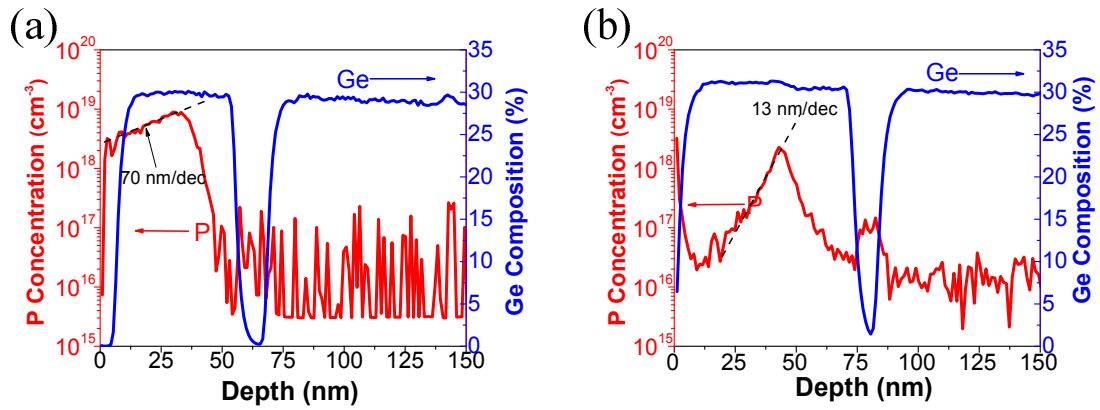


Fig. 4.16 SIMS results of Ge and P profiles of (a) sample #5414 and (b) sample #5613. The phosphorus level at the surface are 2×10^{18} and 2×10^{16} cm⁻³ for sample #5414 and #5613, respectively.

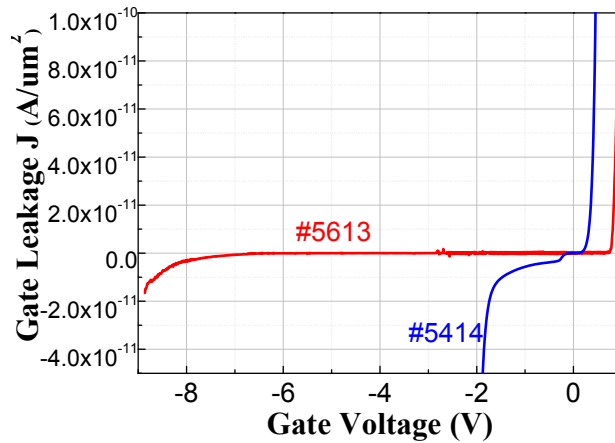


Fig. 4.17 Gate leakage current density at 4 K vs. gate voltage for sample #5414 and #5613, respectively. Pd Schottky gate covered the entire Hall bar shown in Fig. 4.15.

achieved with a much reduced P surface level of 2×10^{16} cm⁻³. This enabled extremely low gate leakage current at negative applied voltage until -7 V. At forward bias, a normal Schottky diode operation was observed at 0.2 and 0.7 V for #5414 and #5613, respectively.

Two wafers (#5737 and #5747) with different setback layer thicknesses (Fig.

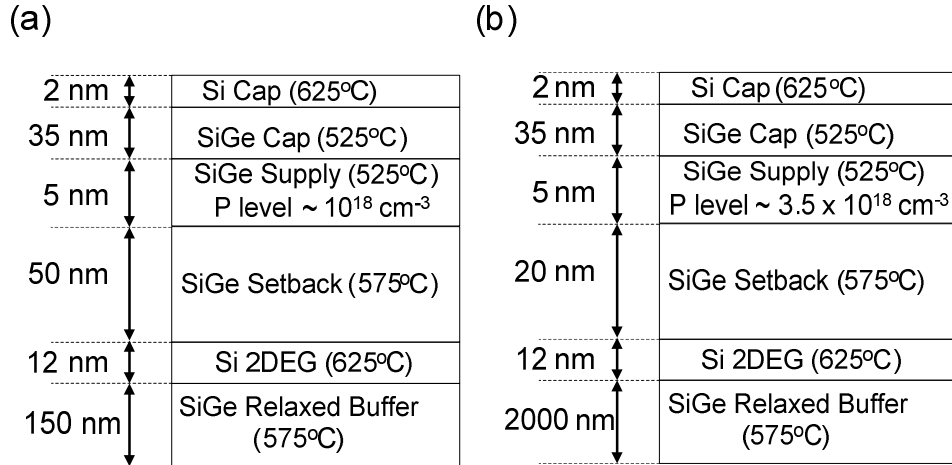


Fig. 4.18 Layer structures of (a) sample #5737 and (b) sample #5747. The phosphorus doping levels are 1×10^{18} and $3 \times 10^{18} \text{ cm}^{-3}$ for (a) and (b), respectively.

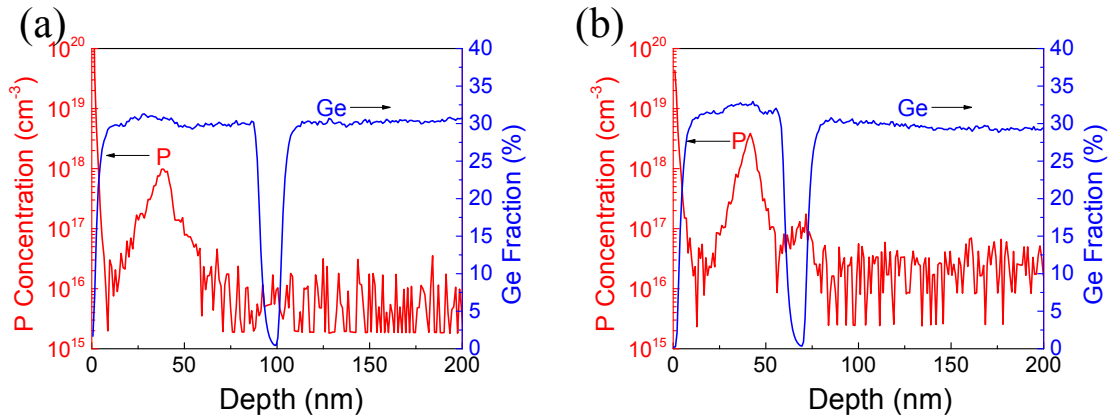


Fig. 4.19 SIMS results of Ge and P profiles for (a) #5737 and (b) #5747. The bump of P in the Si QW layer is thought the artifact of SIMS measurement.

4.18) were grown and Hall bar devices were fabricated with Pd Schottky gates on top, covering the entire Hall bar. The SIMS results of these two wafers confirm the low levels of surface phosphorus ($< 10^{16} \text{ cm}^{-3}$) by low-temperature epitaxy at 525 °C (Fig. 4.19). Thus, effective Schottky gating was enabled with very low gate leakage current of 0.1 nA compared to the drive current of 100 nA (Fig. 4.20(a)).

The electron density vs. gate voltage of #5737 by Pd Schottky gating is shown

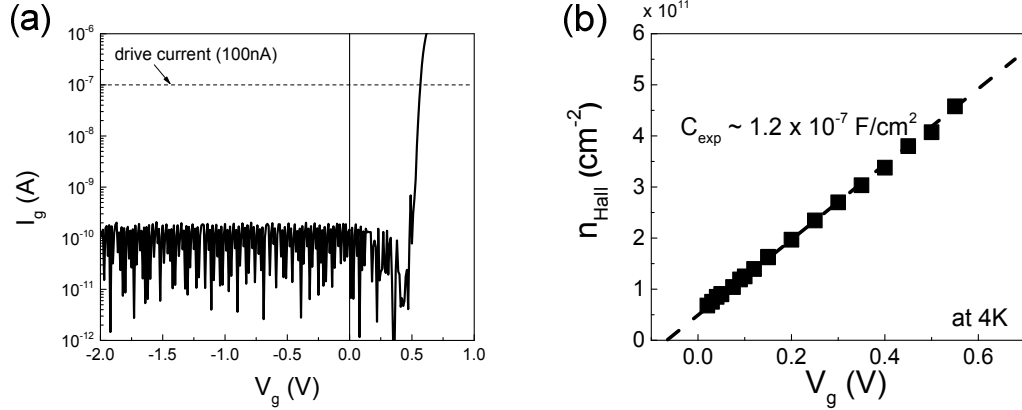


Fig. 4.20 (a) Gate leakage current (I_g) and (b) electron density vs. gate voltage (V_g) for sample #5737 at 4 K. At $V_g = 0.5$ V, a normal forward-bias Schottky diode operation was observed. The drive current for the Hall measurement was 100 nA.

in Fig. 4.20(b). The effective capacitance between the surface and the 2DEG layer can be extracted from the slope of n_{2D} vs. V_g as 1.2×10^{-7} F/cm², which is close the calculated value of 1.3×10^{-7} F/cm² based on a parallel capacitor model. By extrapolating the line to $n_{2D} = 0$, $V_g = -0.06$, V was obtained for full depletion of electrons in the 2DEG layer. However, below $V_g = 0.02$ V, there was no conduction in this sample because of metal-insulator transition (MIT). MIT occurs because of the potential fluctuations from the remote impurities of the supply layer, which creates numerous barriers blocking electron transport at low densities [90]. Thus, conduction ceases.

The mobility vs. density of sample #5737 (setback: 50 nm) and #5747 (setback: 20 nm) are shown in Fig. 4.21. At the same density, the mobility of #5737 is higher than that of #5747 due to the thicker setback layer that separates the ionized impurity and 2DEG. As the density increases, the mobility of both samples increases because of the stronger electron screening. The slopes of mobility vs. density for #5737

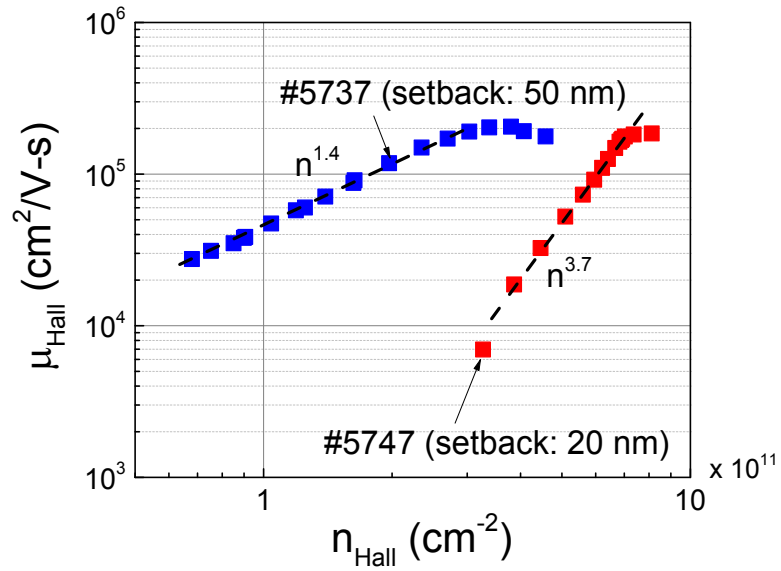


Fig. 4.21 Hall mobility vs. density at 4 K for sample # 5737 (setback: 50 nm) and # 5747 (setback: 20 nm).

and #5747 were extracted as $\mu \propto n^{1.4}$ and $\mu \propto n^{3.7}$, respectively. It is suggested in the mobility models [63, 79, 82] that if the mobility is limited by the remote impurity scattering, the exponent of $\mu \propto n^\alpha$ will be close to 1.5. On the other hand, if the background impurity scattering dominates, the exponent is close to 1. This has been experimentally verified with exponents of 0.5 ~ 1.5 for modulation-doped GaAs 2DEGs [91] and undoped Si 2DEGs [73]. For sample #5737, the mobility is probably limited by the remote impurity scattering, as the exponent is close to 1.5. For sample #5747, the exponent is 3.7, which is much higher than any theoretical numbers. Prior work on Si 2DEGs has also reported an exponent of 2.4, and suggested the inadequacy of the Thomas-Fermi approximation on electron screening as the electrons move closer to the MIT regime [92].

Note that the MIT occurs at 6.5×10^{10} and $3.2 \times 10^{11} \text{ cm}^{-2}$, with mobilities of 30,000 and 7,000 $\text{cm}^2/\text{V-s}$ for #5737 and #5747, respectively. For sample #5737, the mobility at $n_{2D} = 1 \times 10^{11} \text{ cm}^{-2}$ is 45,000 $\text{cm}^2/\text{V-s}$. To our knowledge, this is the highest mobility reported for modulated-doped Si 2DEGs at a density of 10^{11} cm^{-2} - an indication of the high quality of our 2DEG samples. The higher critical density for MIT to occur in #5747 is attributed to its shorter setback layer, leading to stronger effects of potential fluctuations on 2DEG so that the metallic conduction ceases at a higher electron density [89].

There is a saturation in mobility at $n_{2D} = 3.6 \times 10^{11}$ and $7.9 \times 10^{11} \text{ cm}^{-2}$ for #5737 and #5747. Several reasons could be attributed to the maximum mobility, such as parallel conduction in the supply layer [93, 94], or the second subband occupancy in the Si QW layer [95], or the interface roughness scattering [88] at the upper SiGe/Si interface coming from a higher electric field pushing the 2DEG to the interface with a high electron density. In chapter 5, a preliminary analysis will show that, in our 2DEG devices, the electron occupancy of the second subband in the Si QW layer is the main reason for the presence of peak mobility.

Finally, concerning the amazingly high exponent of $\mu \propto n^\alpha$ in sample #5747, we note that when we derived the 2DEG mobility in section 4.2.4, electron tunneling between the Si QW layer and the SiGe supply layer was ignored. However, for a 2DEG with a thin setback layer, such as sample #5747 (20 nm), electron tunneling could occur. When tunneling happens, there might be a parallel conduction channel in the remote supply layer [93], even if the electron density in the supply layer is below the critical density as MIT occurs. Thus, the measured Hall density and mobility do not represent

the true 2DEG characteristics and an elaborate analysis is required [94]. Lu *et al.* reported an upper limit of 2DEG density in an undoped Si 2DEG and suggested that it could be related to the tunneling between the 2DEG and the Si surface layer [96]. However, no further experimental result was presented to support their concept of electron tunneling in a 2DEG structure. Furthermore, exactly how this tunneling would affect electron screening and mobility is not yet known. Thus, a quantitative interpretation of our data of μ vs. n , and the high exponent cannot be made at this time. More work is required in order to understand the effect of tunneling on 2DEG properties.

4.6 Summary

In this chapter, we first reviewed the electrostatics and a mobility model of a Si 2DEG. Then, we demonstrated much improved mobility in Si 2DEGs grown by piping PH_3 separately from the other gases, which reduces the phosphorus background level to below 10^{15} cm^{-2} in epitaxial films grown by our CVD system. A high mobility of $522,000 \text{ cm}^2/\text{V-s}$ without external gating was achieved, which is the highest reported among all un-gated modulation-doped Si 2DEGs grown by CVD.

We then investigated the effects of different layers on the 2DEG properties. The feasibility of using a SiGe virtual substrate for high-quality Si 2DEGs was demonstrated by increasing the thickness of the SiGe buffer layer. Furthermore, the thickness of the Si QW layer was shown to be crucial for the 2DEG mobility due to the detrimental strained relaxation of the Si layer as it is over the critical thickness. A Si QW layer of 9 to 12 nm was suggested for high-mobility Si 2DEGs.

By low-temperature epitaxy, effective Schottky gating on single 2DEG devices was enabled, and an extremely low electron density of $6.5 \times 10^{10} \text{ cm}^{-2}$ was obtained by gating with a mobility of $45,000 \text{ cm}^2/\text{V-s}$ at the important density of $1 \times 10^{11} \text{ cm}^{-2}$. The relation between modulated mobility and density was used to identify the dominant scattering mechanism. It was expected that the remote impurity scattering would be the dominant mechanism at densities below $4 \times 10^{11} \text{ cm}^{-2}$. However, the mobility model could not completely explain our experimental results, particularly the exact numerical dependence of μ on n . A new model to include possible tunneling between 2DEG and the remote supply layer is required in order to accurately explain the 2DEG characteristics in a device with short setback distance.

Chapter 5 Isotopically Enriched ^{28}Si 2DEGs and Inverted Modulation-Doped Si 2DEGs

5.1 Introduction

In 2005, Petta *et al.* demonstrated the first spin-based quantum computing in a double quantum dot device operation in a GaAs two-dimensional electron gas (2DEG) [12]. However, strong spin decoherence exists in a GaAs-based QD because of the hyperfine interactions of electron spins and nuclear spins. Alternatively, for Si QDs, greatly reduced spin decoherence was demonstrated with a longer dephasing time (T_2^*) [13] because of the lower fraction of the only nuclear-spin-carrying isotope of ^{29}Si (4.7 %) [97]. Moreover, ^{29}Si can be reduced by ^{28}Si enrichment [98] and reduced spin decoherence is predicted [99]. Thus, in the first part of this chapter, we present the work concerning the electron transport properties of enriched ^{28}Si 2DEGs.

The second part of this chapter is the demonstration of inverted modulation-doped 2DEGs in silicon with natural isotope abundance, with record high mobility of $470,000 \text{ cm}^2/\text{V}\cdot\text{s}$. This inverted structure is crucial to the realization of a bilayer device of two adjacent 2DEGs with a thin tunneling barrier in between [100]. While a GaAs-based bilayer device has been fabricated successfully by the delta-doping technique [101], there is no experiment reported on a Si bilayer device yet. The major obstacle for the demonstration of a Si bilayer device is the severe surface segregation of n-type dopants, which would reduce the mobility in the bottom channel of Si 2DEG due

to stronger impurity scattering from the n-type dopants in the setback layer. In the second part of this chapter, we investigate the effects of phosphorus segregation on electron transport in an inverted modulation-doped Si 2DEG. By low-temperature epitaxy to suppress phosphorus segregation, an inverted modulation-doped Si 2DEG of high mobility of $470,000 \text{ cm}^2/\text{V-s}$ is presented.

5.2 Isotopically Enriched ^{28}Si 2DEGs

Quantum dots (QDs) containing single electrons are very promising for the realization of spin-based quantum computing in solid-state systems because of their scalability [5] and the mature nature of semiconductor technology. The coherent control over the spin states of two single electrons in a double quantum dot was demonstrated in GaAs for the first time [12]. However, its short dephasing time T_2^* of $\sim 7 \text{ ns}$ of electron spins, due to the severe hyperfine interactions with the host nuclei [11], imposes a lower limit on the speed of gate switching to preserve the quantum phase information before a gate switching operation is completed. To increase the dephasing time of electron spins, silicon has been suggested as a replacement for GaAs because of the very low spin decoherence resulting from its only spin-carrying isotope ^{29}Si of 4.7 % [97]. A much longer T_2^* of $\sim 360 \text{ ns}$ was recently demonstrated in a Si double QDs [13]. With the reduction of ^{29}Si to below 0.01 %, a very long dephasing time has been predicted because of the greatly suppressed hyperfine interactions between electron spins and nuclear spins of ^{29}Si [99].

A 2DEG in an isotopically-enriched ^{28}Si quantum well (QW) was

demonstrated by molecular beam epitaxy (MBE), with the mobility of 55,000 cm²/V-s at density of 3×10^{11} cm⁻² [98]. The reason of its relatively low electron mobility compared to Si 2DEGs of natural abundance and the limiting factor of electron scattering are still unknown. Moreover, there is no report yet on an enriched ²⁸Si 2DEG prepared by CVD. Thus, we study the transport properties of enriched ²⁸Si 2DEGs by CVD and estimate the spin decoherence in this section.

Table 5.1 Layer structures of isotopically-enriched ²⁸Si 2DEGs

Layer	Growth Temp. (°C)	Thickness (nm)	
		Modulation-Doped (Depletion-mode)	Undoped (Enhancement-mode)
Si cap	625	7	3
SiGe cap	575	25	0
SiGe supply (doping level)	575	10 (4×10^{18} cm ⁻³)	(no doping) 60 (#5854) or 150 (#5853)
SiGe setback	575	25	
Si quantum well	625	16	9*
SiGe buffer	575	110	150

* ²⁸Si was only enriched in the Si quantum well.

The preparation of enriched ²⁸Si 2DEG samples was similar to the steps described in chapter 4, except that a specialized silane of enriched ²⁸Si (provided by Voltaix Inc.) was used as a gas precursor. After the cleaning steps, relaxed SiGe substrates were loaded into the CVD reactor for epitaxial growth. A SiGe buffer layer of 100 ~ 150 nm was first grown at 575 °C, followed by a strained-Si layer (2DEG layer)

at 625 °C, a SiGe setback layer at 575 °C, a n-type SiGe supply layer at 575 °C, a SiGe cap layer at 525 °C, and a Si cap layer at 625 °C (Table 5.1). There are two sets of samples in this section. First, a depletion-mode device of modulation-doped 2DEG with ^{28}Si enriched throughout the entire epitaxial growth (including Si and SiGe epitaxial layers) was fabricated. For enhancement-mode samples, the supply layer was grown without n-type doping and ^{28}Si was only enriched in the Si QW layer.

5.2.1 Reduction of Spin-Carrying Isotope ^{29}Si by ^{28}Si Enrichment

The concentrations of three isotopes, ^{28}Si , ^{29}Si , and ^{30}Si , and Ge vs. depth in a modulation-doped enriched ^{28}Si 2DEG device are shown in Fig. 5.1. Below the growth interface at 185 nm depth, the fractions of ^{28}Si , ^{29}Si , and ^{30}Si are 92 %, 4.7 %, and 3.3 %, respectively, which are identical to the compositions of the natural isotopic

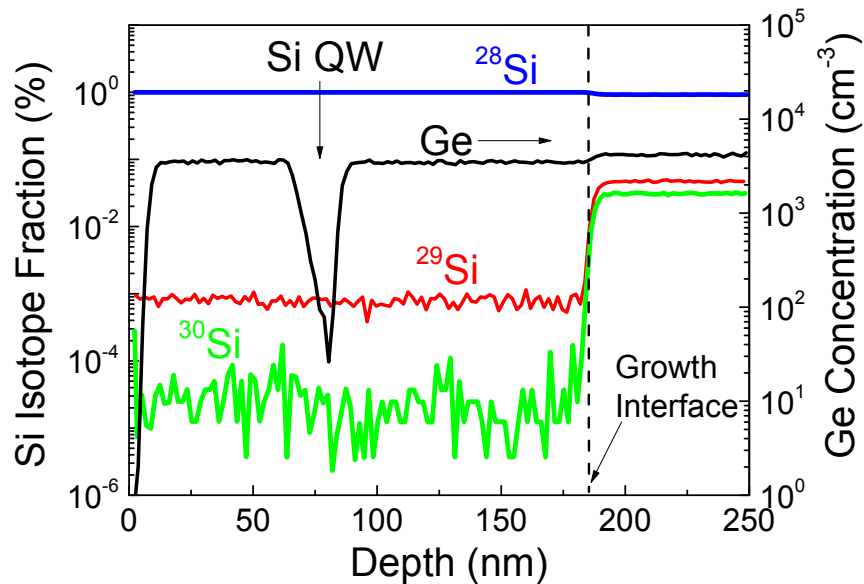


Fig. 5.1 Three isotopes ^{28}Si , ^{29}Si , and ^{30}Si vs. depth in 2DEG structure with Ge as an indicator by SIMS measurements. The growth began at a depth of 185 nm and Si QW is at a depth of 75 nm.

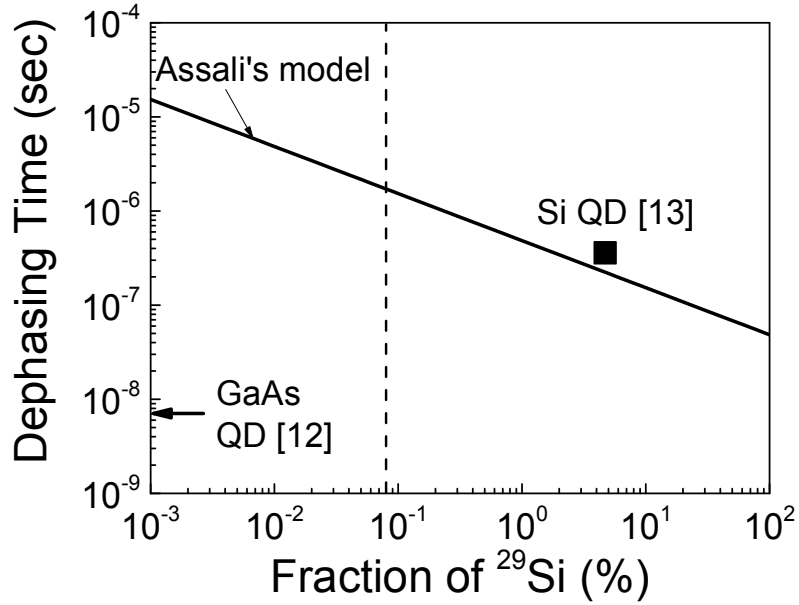


Fig. 5.2 Dephasing time vs. ^{29}Si fraction. Solid line is the model prediction, the solid square is the experimental result in Si QD [13], and the vertical dash line represents the fraction of ^{29}Si in our enriched ^{28}Si 2DEGs. Dephasing time of GaAs QDs [12] is also presented for comparison.

abundance [97]. For Si and SiGe epitaxial layers grown with silane of enriched ^{28}Si , the fractions for those three isotopes became 99.72 %, 0.08 %, and 0.002 %, respectively. The enrichment factors, defined as the ratios of ^{28}Si to ^{29}Si and ^{28}Si to ^{30}Si , were increased from 20 to 1250 (i.e., 60 times enhancement), and 27 to 50,000 (i.e., 2000 times enhancement), respectively.

We now estimate the potential effects of ^{28}Si enrichment on the spin decoherence in Si QDs. By the enrichment of ^{28}Si , the spin decoherence of QD electrons from the nuclear spins of ^{29}Si can be greatly suppressed. This would reduce the dephasing time (T_2^*), which is dominated by the hyperfine interactions between nuclear

spins and electron spins. Assuming 10^5 nuclei in a Si QD of $100 \text{ nm} \times 100 \text{ nm}$, Assali *et al.* proposed a numerical model to estimate the dephasing time in Si [99]

$$T_2^* = \frac{\hbar}{4.3e\sqrt{10^5 r}} \times 10^{11} \quad (5.1)$$

where e is the electron charge and r is the fraction of ^{29}Si . The predicted dephasing time versus r was shown in Fig. 5.2 and compared with experimental results of a GaAs QD and a Si QD of natural abundance. Maune *et al.* reported the first dephasing time of 360 ns in Si double QDs of natural abundance [13], which is 50 times longer than that in a GaAs QD and very close to Assali's prediction. In our sample, the fraction of ^{29}Si was purified by a factor of 20 to 0.08% and the dephasing time is expected to be 2 μs , two orders of magnitude longer than that of a GaAs QD and 6 times longer than that of a Si QD of natural abundance. According to the model, if ^{29}Si can be reduced to 10 ppm, the decoherence can be further reduced with T_2^* longer than 10 μs .

5.2.2 Magneto-Transport Properties of a Modulation-Doped Enriched ^{28}Si 2DEG

For the depletion-mode device (#5514), Hall electron density at 4 K was $4 \times 10^{11} \text{ cm}^{-2}$ with mobility of $399,000 \text{ cm}^2/\text{V}\cdot\text{s}$. The longitudinal (R_{xx}) and transverse (Hall) resistances (R_{xy}) were also measured at 0.3 K with the magnetic field up to 8 T (Fig. 5.3). The onset of Shubnikov-de Haas (SdH) oscillations in R_{xx} occurs at 0.4 T. The spin splitting, which occurs because of the associated Zeeman energy difference exceeding the Landau level broadening, occurs at 0.75 T with a filling factor of $\nu = 24$. The revelation of the two-fold degeneracy from two valleys of density of states was observed

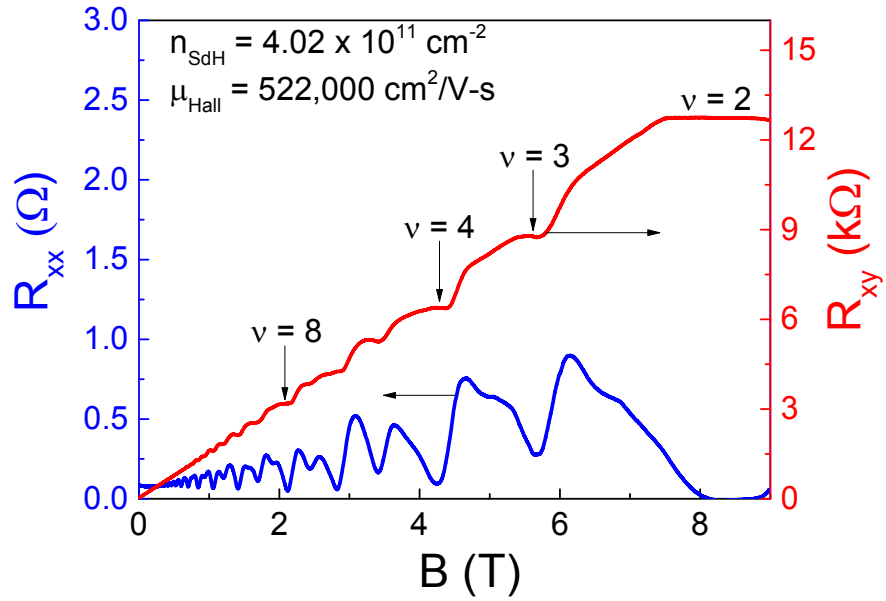


Fig. 5.3 Magneto-resistances of depletion-mode enriched ^{28}Si 2DEG device measured at 0.3 K. Electron density ($4.02 \times 10^{11} \text{ cm}^{-2}$) and mobility ($522,000 \text{ cm}^2/\text{V-s}$) were extracted from the periods of Shubnikov-de Haas oscillations in longitudinal resistance (R_{xx}) vs. $(1/B)$ and its value at zero field.

at 1.9 T with $\nu = 9$. For Hall resistance (R_{xy}), the quantum Hall structures can be resolved at $B = 0.7$ T with the filling factor of $\nu = 24$ and clear plateaus were observed at $\nu = 2, 4, 8$, etc. The two-dimensional electron densities extracted from SdH oscillations and low-field Hall resistance were 4.02 and $4.18 \times 10^{11} \text{ cm}^{-2}$, respectively, showing that parallel conduction is insignificant. The electron mobility of this device at 0.3 K was $522,000 \text{ cm}^2/\text{V-s}$, with an associated mean free path of $6 \mu\text{m}$, which we believe is the highest reported for any modulation-doped Si 2DEG grown by CVD, regardless of ^{28}Si enrichment. In previous work on isotopically enriched ^{28}Si , the highest reported mobility was $55,000 \text{ cm}^2/\text{V-s}$ in a MBE-grown 2DEG. Our results established the extremely high quality in the isotopically enriched samples.

5.2.3 Gating of Enhancement-Mode Enriched ^{28}Si 2DEGs

For quantum dot devices, a short distance between the surface and 2DEG layer is preferred for fine gate control. Thus, we chose shallow 2DEGs with the SiGe setback layer < 150 nm thick. Two enhancement-mode devices, with undoped enriched ^{28}Si used only in the Si QW layer, were made, without any n-type dopants, and with a SiGe setback layer of 60 (#5854) and 150 nm (#5853). The growth parameters and layer structures are listed in Table 5.1. Al_2O_3 of 90 nm was deposited at 300 °C over the entire device. A metal gate of Cr/Au with a Hall bar shape was deposited on top of Al_2O_3 (Fig. 5.4). In these undoped enhancement-mode devices, there cannot be parallel conduction in an n-type supply layer. Aside from this, since the Si surface layer was thin (< 3 nm), the quantum states in that layer are higher than the Fermi level, eliminating the potential parallel conduction at the surface. Furthermore, considering the intimate proximity with the Si/ Al_2O_3 interface, the surface conduction is negligible because of the strong scattering from the interface impurity and roughness compared to the conduction in the 2DEG layer. Thus, the measured Hall density and mobility are considered to reflect 2DEG transport properties in this work.

With a metal gate of Cr/Au on top of 90-nm Al_2O_3 (Fig. 5.4), the electron

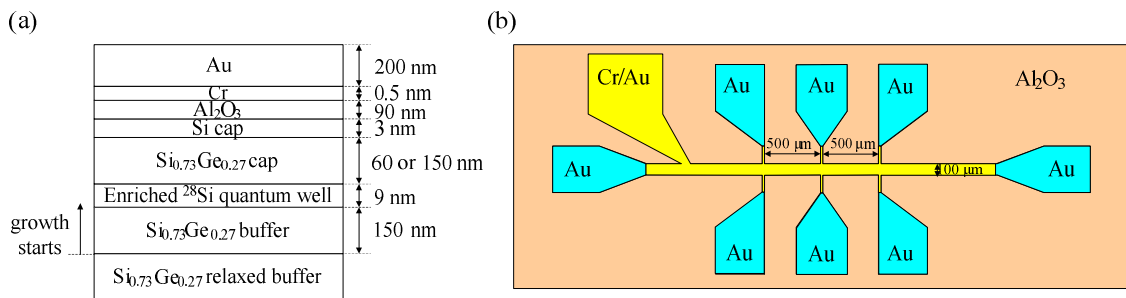


Fig. 5.4 (a) The layer structure of enhancement-mode devices of Si 2DEGs, and (b) the top view of the Hall bar geometry.

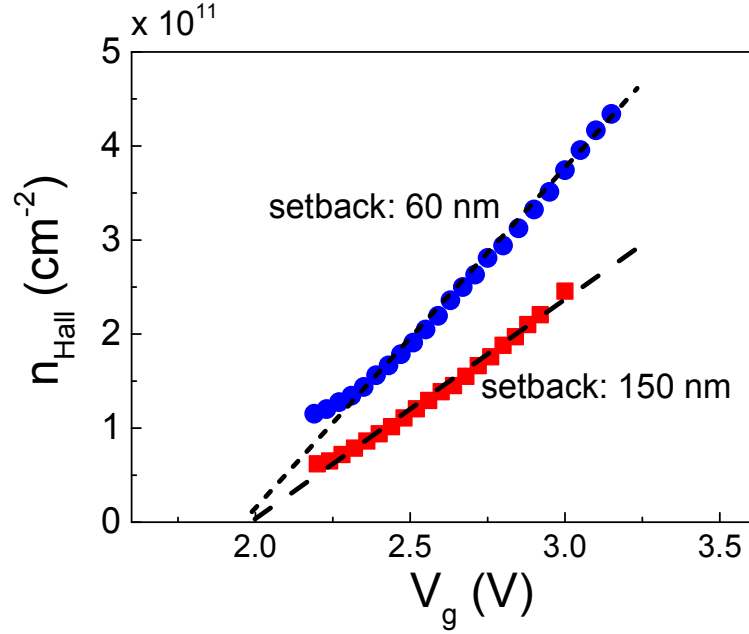


Fig. 5.5 Electron density vs. gate voltage by Hall measurement at 4 K for enhancement-mode devices of enriched ^{28}Si 2DEG with a SiGe setback layer of 60 and 150 nm. The slopes represent the effective capacitance between a Cr/Au gate and 2DEG.

density and mobility in the 2DEG layer can be modulated and the dominant scattering mechanisms could be verified by checking μ vs. n_{2D} in relation to different thicknesses of the SiGe setback layer (60 and 150 nm). The electron density vs. gate voltage of those two samples was shown in Fig. 5.5. The capacitances extracted from the slopes are $5.8 \times 10^{-8} \text{ F/cm}^2$ and $4.1 \times 10^{-8} \text{ F/cm}^2$ for the setback layer of 60 and 150 nm, respectively, within 5% of the values calculated with a parallel-plate capacitor model. The lowest densities are 1.1 and $0.6 \times 10^{11} \text{ cm}^{-2}$ at $V_g = 2.2 \text{ V}$, which we believed is the lowest density among all reported enriched ^{28}Si 2DEGs. The extrapolation of n_{2D} vs. V_g to zero density gives the threshold voltage (V_T) approximately 2 V. Below $V_g = 2.2 \text{ V}$, however, there was no conduction in the 2DEG channel because of the metal-insulator transition (MIT) [90]. By assuming the threshold voltage is dominated by impurity charge (Q_{int}) at

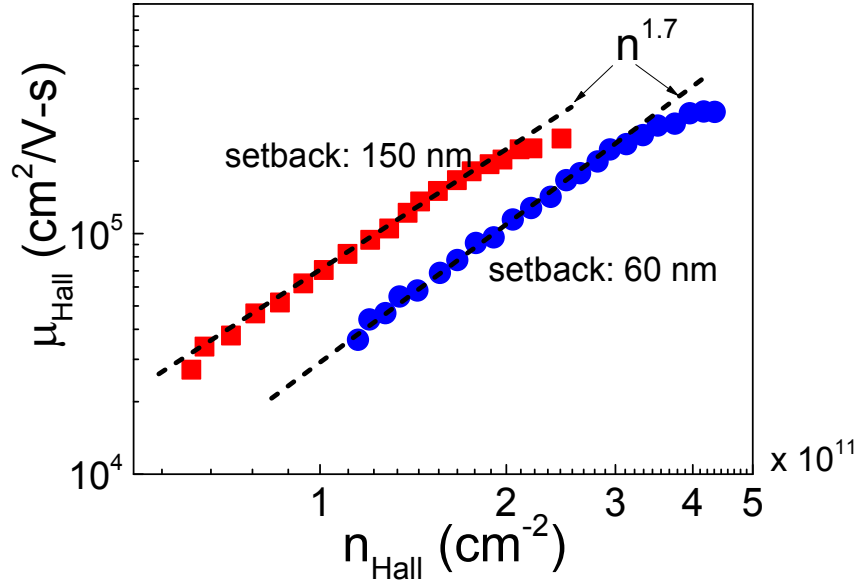


Fig. 5.6 Hall mobility vs. density for enhancement-mode devices of enriched ^{28}Si 2DEG with a SiGe setback layer of 60 and 150 nm at 4 K.

the Si/Al₂O₃ interface, a simple estimation can be made with $N_{int} = Q_{int}/e = C_{ALO} \times V_T / e$ on the order of 10^{12} cm^{-2} , where C_{ALO} is the capacitance ($7.9 \times 10^{-8} \text{ F/cm}^2$) of 90-nm Al₂O₃ dielectric layer assuming its relative dielectric constant is 8.

In Fig. 5.6, electron mobility vs. density at 4 K for these enhancement-mode devices is illustrated. For the device with a 150-nm SiGe setback layer, the lowest density is $6.2 \times 10^{10} \text{ cm}^{-2}$ with mobility of $28,000 \text{ cm}^2/\text{V-s}$. Below this critical density, electron conduction ceased because MIT occurs. For both devices, the mobility scales with the density as $\mu \propto n^{1.7}$. Based on previous work [82, 91], if the 2DEG is limited by the remote impurity scattering, then $\alpha = 1.5$. Thus, we concluded that the major source of electron scattering in these enriched ^{28}Si 2DEG devices is remote impurities at the Si/Al₂O₃ interface.

5.3 Inverted Modulation-Doped Si 2DEGs

In chapter 4, the remote impurity charges in the supply layer were suggested to be the dominant scattering sources in a modulation-doped device of Si 2DEG, with the supply layer on top of the Si QW layer. Due to a fast turn-on, the level of n-type dopants is low in the setback layer, and the effects of impurity scattering between the doped layer and 2DEG is usually ignored. For inverted structure (Fig. 5.7), with the supply layer below the 2DEG layer, due to the severe surface segregation of n-type dopants, the resulting high level would lead to stronger remote impurity scattering and a greatly reduced mobility. Furthermore, P segregates into the Si QW layer, resulting in high P background levels there (Table 5.2 or Fig. 5.8), which would reduce the 2DEG mobility further. While a sharp arsenic turn-off by ion implantation for the bottom n-type doping layer in an inverted Si 2DEG device was reported [102], the mobility was limited by the defects induced during implant process and the quality of the re-growth interface. Furthermore, high temperature annealing is required to activate the dopants

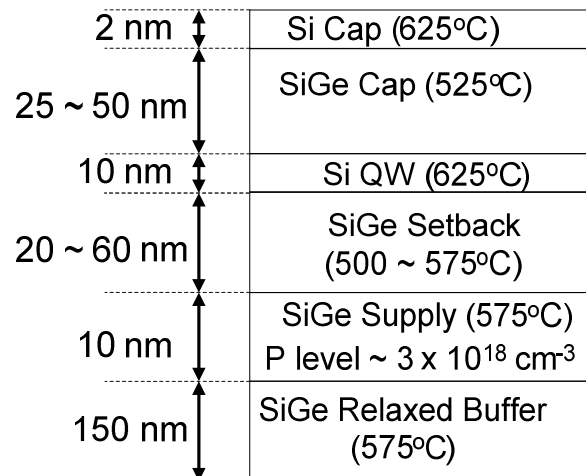


Fig. 5.7 Typical layer structure of an inverted modulation-doped Si 2DEGs. The SiGe supply layer of phosphorus modulation-doping is below the 2DEG layer (Si QW).

and remove the defects by implant, which would induce strain relaxation and increase the thermal budget for the subsequent processing steps. By low-temperature epitaxy (chapter 3), the phosphorus segregation can be significantly reduced with a sharp turn-off, enabling a low level in the setback layer. Thus, sample #5457, #5850, and #5630. P turn-off slopes of these three samples are 40, 14, and 8 nm/dec, respectively. The setback layer thicknesses between the phosphorus peak level and the lower Si/SiGe heterojunction are 20, 20, and 33 nm for those three in the final part of this thesis, we investigate the effect of phosphorus segregation on 2DEG characteristics and present the highest reported mobility of 470,000 cm²/V-s for all inverted modulation-doped Si 2DEGs.

5.3.1 Effects of Phosphorus Turn-Off Slope on 2DEG Mobility

To investigate the effects of phosphorus segregation on 2DEG properties in an inverted structure, three samples of different phosphorus turn-off slopes (40, 14, and 8 nm/decade) were grown at different temperatures. The details of the layer structures are listed in Table 5.2 and the associated SIMS results are illustrated in Fig. 5.8. For those three samples, the thickness of the setback layer is defined as the distance between the phosphorus peak and the lower Si/SiGe heterojunction. Hall electron density and mobility measured at 4 K are plotted versus the phosphorus turn-off slope in Fig. 5.9.

The Hall electron densities of sample #5457, #5850, and #5630 are $3.8 \times 10^{12} \text{ cm}^{-2}$, $7 \times 10^{11} \text{ cm}^{-2}$, $1.8 \times 10^{11} \text{ cm}^{-2}$, respectively. As P turn-off slope increases, there is more phosphorus in the SiGe setback layer, which would effectively reduce the setback layer thickness by transferring electrons at shorter distances. Furthermore, high

P background levels in the Si QW layer might contribute more electrons in the 2DEG layer. Thus, with the same setback layer thickness of 20 nm, the density of #5457 with P turn-off slope of 40 nm/dec is higher than that of #5850 with P turn-off slope of 12 nm/dec. For #5630 of a thicker setback layer, the P turn-off slope is 8 nm/dec and the P level is very low (below the detection limit), so the electron density is less than those of #5457 and #5850.

Table 5.2 Layer structures of sample #5457, #5850, and #5630 for study of the effects of P turn-off slope on 2DEG characteristics in an inverted modulation-doped structure.

Sample #	5457	5850	5630
Si cap (nm) @ 625°C	5	3	2.5
SiGe cap (nm) @ 575°C	46	38	50
Si QW (nm) @ 625°C	12	11	11
P level in Si QW	$0.6 \sim 2 \times 10^{18} \text{ cm}^{-3}$	$1 \sim 2 \times 10^{17} \text{ cm}^{-3}$	below $5 \times 10^{15} \text{ cm}^{-3}$ (SIMS limit)
SiGe setback (nm)	20	20	33
P turn-off slope	40 nm/dec	14 nm/dec	8 nm/dec
growth temperature	575 °C	525 °C	500 °C
P Peak level (cm^{-3})	4.8×10^{18}	3.3×10^{18}	4.6×10^{18}
SiGe buffer (nm) @ 575°C	160	125	170

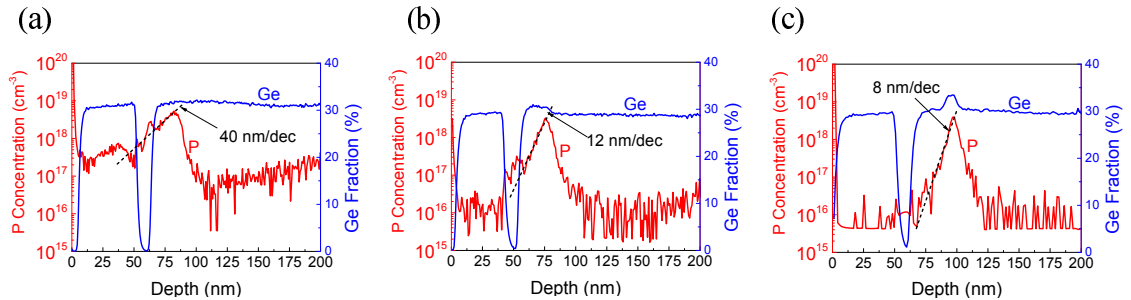


Fig. 5.8 P and Ge profiles of sample #5457, #5850, and #5630. P turn-off slopes of these three samples are 40, 14, and 8 nm/dec, respectively. The setback layer thicknesses between the phosphorus peak level and the lower Si/SiGe heterojunction are 20, 20, and 33 nm for those three samples.

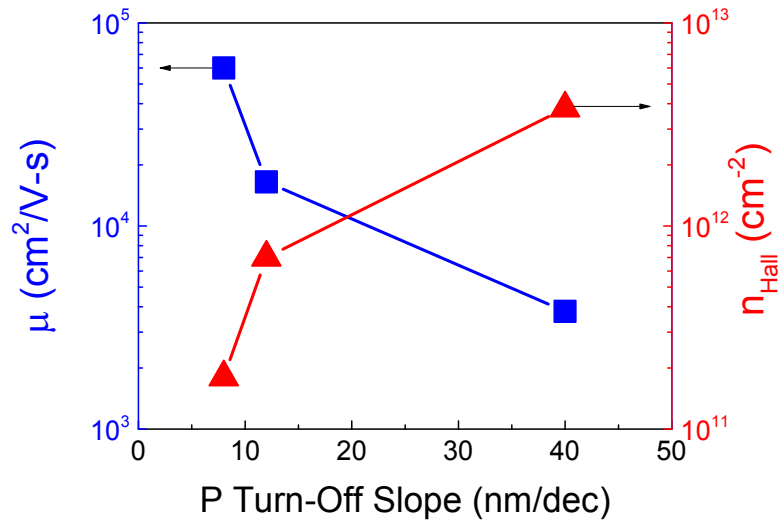


Fig. 5.9 Hall density and mobility vs. P turn-off slope for sample #5457 (40 nm/dec), #5850 (14 nm/dec), and #5630 (8 nm/dec). A corrected electron density was calculated by Poisson's equation to compensate the effect of the thicker SiGe setback layer in sample # 5630.

2DEG mobility is also affected greatly by phosphorus turn-off slope (Fig. 5.9). With a fast phosphorus turn-off slope of 8 nm/dec in sample #5630, the mobility is 60,000 cm²/V-s, 20 times higher than that of sample #5457 with a slow slope of 40 nm/dec. For sample #5457, even though electron screening is expected to be stronger than sample #5630 because of the higher electron density ($3.8 \times 10^{12} \text{ cm}^{-2} \gg 1.8 \times 10^{11} \text{ cm}^{-2}$), the mobility is actually much lower. This is attributed to the high level of phosphorus in the setback layer because of a slow phosphorus turn-off, introducing stronger remote impurity scattering for 2DEG. Furthermore, for the sample of a slow P turn-off such as #5457, the resulting high P level of 10^{18} cm^{-3} in the Si QW layer could cause stronger background impurity scattering. Both remote and background impurity scattering affect the 2DEG mobility in the inverted modulation-doped Si 2DEGs with slow P turn-off. Thus, a fast P turn-off must be used for high-mobility 2DEGs.

5.3.2 Effects of Remote Impurity at the Si/Al₂O₃ Interface on Mobility

In this section, we study the effect of the impurity charges at the Si/Al₂O₃ interface. Unlike a top modulation-doped Si 2DEG with ionized impurities in the supply layer to screen the remote charges at the Si surface, in an inverted structure, the remote scattering effect of the Si surface charges must be considered because of the absence of an n-type doping layer between the surface and 2DEG. If the charge density at the surface is higher than the remote impurity charge in the bottom supply layer in an inverted 2DEG device, presumably, the mobility would be largely affected by those unscreened surface charges [89]. By reducing the surface charge density or the distance between the surface and 2DEG [73], the scattering is expected to be weaker.

Table 5.3 Layer structures of sample #5877 and #5630 for study of the effects of impurity charges at the Si/Al₂O₃ interface on 2DEG mobility.

Sample #	5877	5630
Si cap (nm) @ 625°C	3	2.5
SiGe cap (nm) @ 575°C	26	50
Si QW (nm) @ 625°C	11	11
P level in QW (cm ⁻³)	below 5 × 10 ¹⁵	below 5 × 10 ¹⁵
SiGe setback (nm)	62	33
P turn-off slope	13 nm/dec; @ 525 °C	8 nm/dec; @ 500 °C
P Peak level (cm ⁻³)	2.5 × 10 ¹⁸	4.6 × 10 ¹⁸
SiGe buffer (nm) @575°C	115	170

Hall bar devices with a Cr/Au/Al₂O₃ gate stack on top of inverted modulation-doped Si 2DEGs (Fig. 5.4) were fabricated to investigate the effect of the

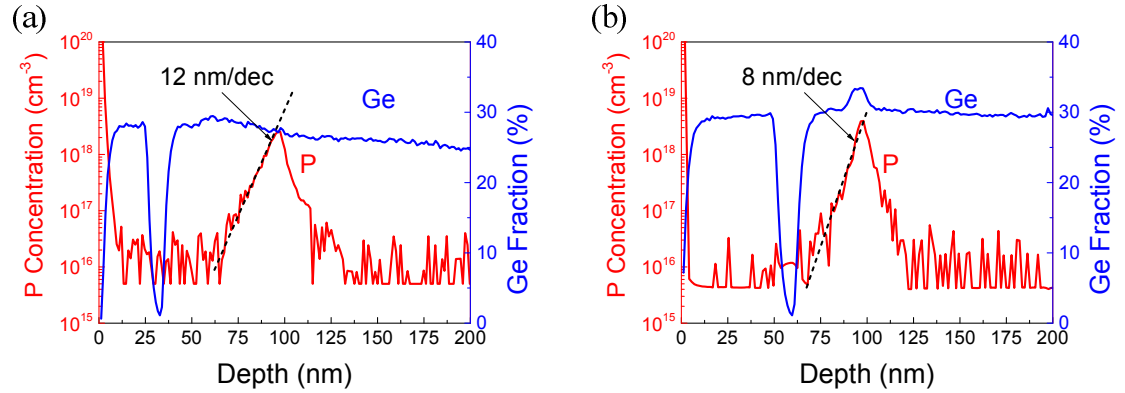


Fig. 5.10 SIMS profiles of (a) #5877 and (b) #5630 of different top SiGe cap thicknesses.

surface charges on the 2DEG transport properties. Two samples of different thicknesses of top SiGe cap layer, which separates the surface charges and 2DEG were grown (Table 5.3). SIMS profiles of these two samples are plotted in Fig. 5.10. The P turn-off slopes for those two samples are different because of the different growth temperatures. The levels of phosphorus background are as low as the SIMS detection limit, of $4 \times 10^{15} \text{ cm}^{-3}$. Therefore, the background impurity scattering is not considered the dominant scattering mechanism. Mobility vs. density for these two devices at 4 K by gating is plotted in Fig. 5.11. The mobility of #5877 (26-nm SiGe cap) is much lower than that of #5630 (50-nm SiGe cap), which is attributed to the stronger scattering from the remote scattering of surface charges with a shorter distance for the 2DEG to the surface. Furthermore, the bottom SiGe setback layer of #5877 is two times larger than that of #5630. The remote impurity scattering at the bottom supply layer is considered much weaker than that in #5630. Thus, we believe the mobility is dominated by the remote impurity scattering from the Si/Al₂O₃ interface. In addition, the critical density for metal-insulator transition (MIT) to occur in #5877 is higher, which also implies the

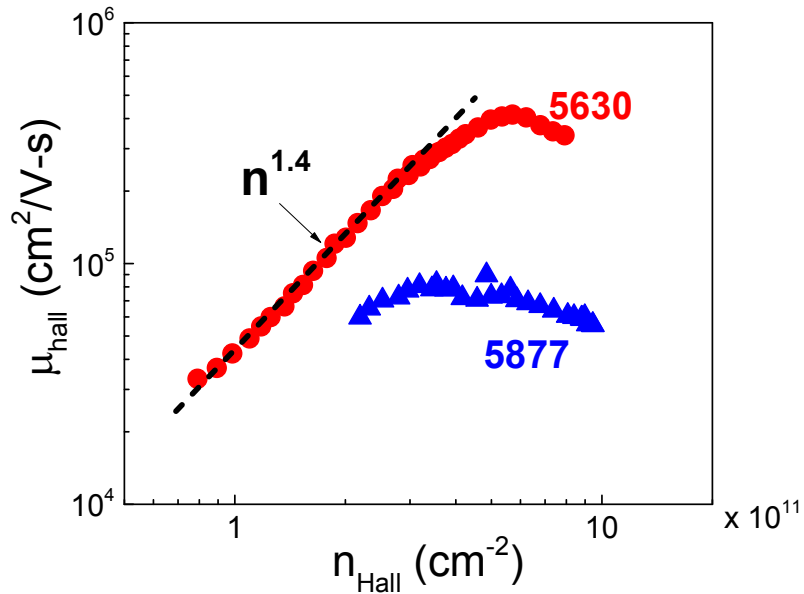


Fig. 5.11 Hall mobility vs. density at 4 K for sample #5630 (50 nm from the 2DEG to the surface) and #5877 (26 nm from the 2DEG to the surface) for a comparison of the effect of upper SiGe cap layer thickness.

stronger remote scattering from the Si/Al₂O₃ interface.

For #5630, an extremely low density, as low as $7.5 \times 10^{10} \text{ cm}^{-2}$ with mobility of $33,000 \text{ cm}^2/\text{V-s}$, was achieved by gating. Alternatively, very high mobility of $420,000 \text{ cm}^2/\text{V-s}$ at 4 K was achieved at density of $5.6 \times 10^{11} \text{ cm}^{-2}$. The levels of the lowest density and the highest mobility in this inverted modulation-doped 2DEG device are comparable to those of the top doped 2DEGs, an indication of the effectiveness of low-temperature epitaxy, which enables low levels of phosphorus in the setback layer and then greatly reduces the impurity scattering. The peak mobility at the high density of $6 \times 10^{11} \text{ cm}^{-2}$ for #5630 could be attributed to the interface roughness scattering [88] or parallel conduction [94, 96]. We will present our analysis in the next section.

5.3.3 Second Subband Occupancy

In a gated device, a maximum in mobility was observed at the density of mid- 10^{11} cm^{-2} in GaAs 2DEGs because of the interface roughness scattering [88] or parallel conduction [94, 96]. For an enhancement-mode Si 2DEG device, the interface roughness scattering was suggested by Huang *et al.* to account for the presence of peak in the mobility [73]. While their results could be fit by a model with several adjustable parameters, it was suggested that in modulation-doped GaAs 2DEGs, the contribution of parallel conduction in other channels such as the doped layer or the second subband in the QW layer would dominate over the interface roughness scattering [63]. This was confirmed by the experimental results of Shubnikov-de Haas oscillations, showing the presence of the parallel conduction in GaAs 2DEGs [103, 104, 105]. Some of the gated devices in this work showed maximum mobility. Thus, we present the analysis of sample #5630 with a peak mobility at density of 6×10^{11} cm^{-2} (Fig. 5.11) and report the first experimental observation of second subband occupancy in a Si 2DEG.

First, Hall density (n_{Hall}) and mobility (μ_{Hall}) vs. gate voltage at 0.3 K of sample #5630 is shown in Fig. 5.12. The device is conducting at $V_g > 1.8$ V with a threshold voltage of 1.45 V by extrapolating n_{Hall} vs. V_g to $n_{Hall} = 0$ (red dash line in Fig. 5.12). Between 1.45 V and 1.8 V, there was no conduction because of the metal-insulator transition. When the channel conducts, the Hall electron density increases with gate voltage. The extracted slope of the Hall density gives the effective capacitance of 6×10^{-8} F/cm² between the Cr/Au gate and the 2DEG layer, which is close to the calculated value of 5.8×10^{-8} F/cm², based on the parallel capacitor model. Note there is a kink in n_{Hall} at $V_g = 3.4$ V, beyond which the predicted density (red dash line in Fig. 5.12 (a)) is

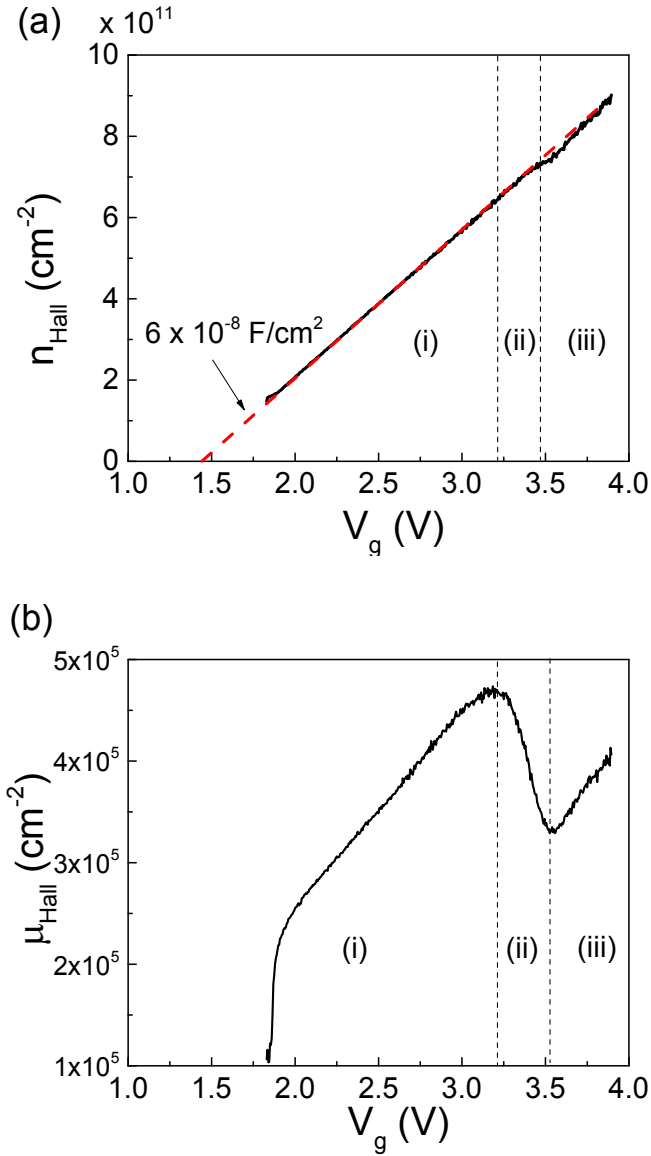


Fig. 5.12 (a) Hall density and (b) Hall mobility at 0.3 K vs. V_g of sample #5630. The onsets of the intersubband scattering and second subband occupancy occurs at $V_g = 3.2 \text{ V}$ and 3.5 V , respectively. In region (i), only the first subband is populated. For region (ii), some electrons in the first subband scatter into and are trapped in the localized states, so the mobility drops. In region (iii), electrons reside in both the first and second subbands, so that the measured Hall mobility increases with electron density because of stronger screening.

actually larger than the measured Hall density (black solid line in Fig. 5.12 (a)). The kink of the Hall density was first reported in a GaAs 2DEG by Störmer *et al.* and

intersubband scattering between the first and the second subbands was suggested to account the kink of the measured Hall density.

A parallel conduction model including the conduction channels in the first and second subbands [79] is used here to help understand the intersubband scattering. With the onset of the occupancy in the second subband of the Si QW layer, the measured Hall density and mobility actually represent the mixed results of parallel conduction in the first and second subbands as follows:

$$n_{Hall} = \frac{(n_1\mu_1 + n_2\mu_2)^2}{n_1\mu_1^2 + n_2\mu_2^2}, \quad (5.1)$$

$$\mu_{Hall} = \frac{n_1\mu_1^2 + n_2\mu_2^2}{n_1\mu_1 + n_2\mu_2}. \quad (5.2)$$

where n_1 and n_2 are the two-dimensional electron densities in the first and second subbands, and μ_1 and μ_2 represent the mobilities in the first and second subband, respectively.

For region (i) in Fig. 5.12, before the onset of the intersubband scattering (i.e. $V_g = 3.2$ V), there exists only one subband. We assume $n_2 = 0$ in this region and n_{Hall} and μ_{Hall} represent n_1 and μ_1 , respectively. In this region, as V_g increases, the electron density increases, leading to stronger electron screening on ionized impurity scattering and enhanced electron mobility. 2DEG mobility is plotted versus density in Fig. 5.13. The mobility scales with the Hall electron density as $\mu \propto n^{1.4}$ for the density below 6×10^{11} cm⁻². The exponent of 1.4 suggests that the remote impurity scattering is the dominant mechanism in this sample [79, 82]. Note that at the density below 2×10^{11}

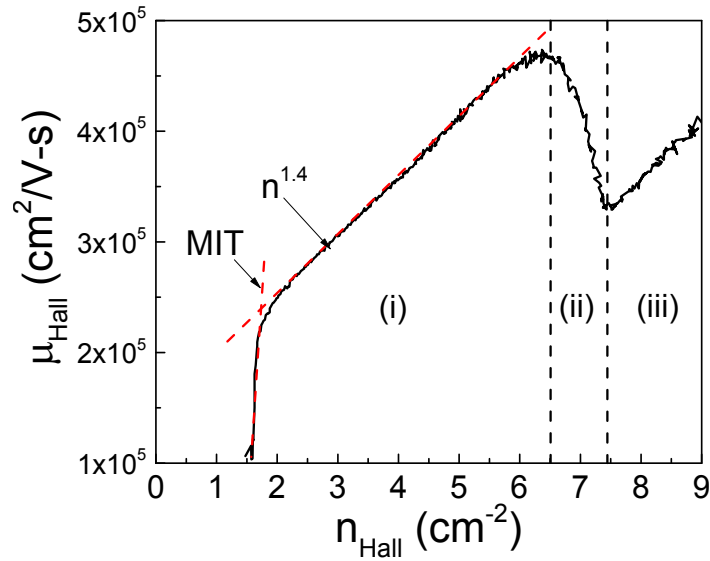


Fig. 5.13 Hall mobility vs. density at 0.3 K of sample #5630.

cm^{-2} , the mobility drops sharply because of the MIT [106].

In region (ii) ($3.2 \text{ V} < V_g < 3.5 \text{ V}$), when V_g increases, the mobility drops from the peak value of $470,000 \text{ cm}^2/\text{V-s}$ to a minimum of $330,000 \text{ cm}^2/\text{V-s}$ with a 30 % decrement (Fig. 5.12 (b)). On the other hand, the Hall density is unaffected in this region (Fig. 5.12(a)). This is surprising because the expected stronger electron screening with V_g would enhance the mobility further. This discrepancy could be explained by the presence of intersubband scattering [103, 105]. When V_g increases, the Fermi level (E_F) is raised and approaches the energy level of the second subband. Despite E_F still below the level of the second subband, the levels of the localized states created by the potential fluctuations of the remote supply impurities could be below E_F in practice. Thus, electrons in the first subband may scatter into and be trapped in those localized states. This additional scattering reduces the 2DEG mobility in the first subband.

To quantitatively explain this argument, we assume there are two conduction channels of electrons in region (ii): the first subband and the localized states of the second subband. Since electrons in the localized states are trapped, we assume $\mu_{\text{local}} = 0$, so n_{Hall} and μ_{Hall} in Eqs. (5.1) and (5.2) represent n_1 and μ_1 , respectively. While n_{Hall} ($= n_1$) increases with V_g , μ_{Hall} drops as V_g increases (Fig. 5.12 (b)). Since $\mu_{\text{local}} = 0$, the measured Hall mobility represents the true 2DEG mobility in the first subband. With the presence of the localized states, electrons in the first subband can scatter into those localized states and be trapped, so μ_{Hall} ($= \mu_1$) drops.

In region (iii), as E_F is lifted further by increasing V_g , the localized states are filled and mobile electrons start to populate the second subband. n_{Hall} and μ_{Hall} represent the combined density and mobility of the first and second subbands following Eqs. (5.1) and (5.2). Since the FFT spectrums of R_{xx} from this sample were too noisy, a quantitative measure of the population process in the first and second subbands is not possible. However, following Störmer's arguments, we assume that when the Fermi level enters the second subband, n_2 increases with V_g and n_1 is constant [103]. For μ_1 and μ_2 , both increases with V_g because of stronger screening by more populated electrons in the second subband. Since both μ_1 and μ_2 could be functions of n_2 , it is not possible to solve them simultaneously without the information of the density in the second subband.

Here, we present a simplified analysis of two channel conduction in region (iii). Assuming above $V_g = 3.5$ V (Fig. 5.12 (b)), the first subband and the localized states of the second subband are fully populated. When V_g increases, electrons are injected into the second subband and the relationship of n_2 and V_g follows a simple parallel-plate capacitor model. Thus, above 3.5 V, n_2 increases from zero with an

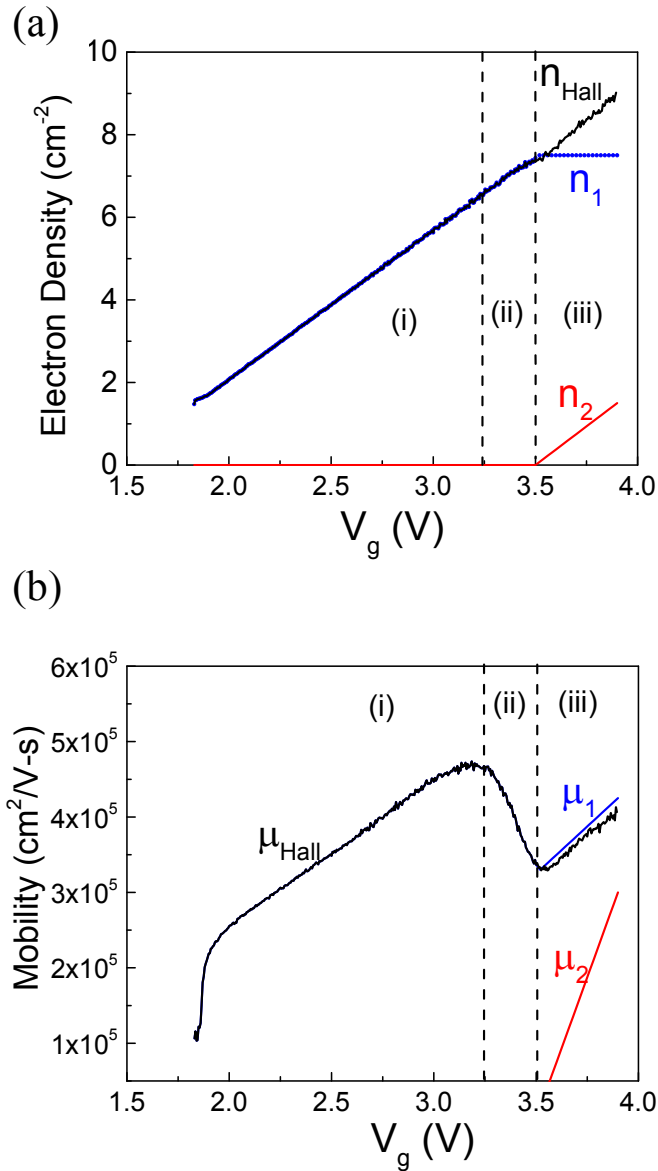


Fig. 5.14 (a) Hall density and (b) Hall mobility at 0.3 K vs. V_g of sample #5630. In region (i) and (ii), n_{Hall} and μ_{Hall} represent n_1 and μ_1 , respectively. For region (iii), assuming n_2 increases from zero with V_g ($V_g = 3.5$ V) by a simple parallel capacitor model, and n_1 is constant, μ_1 , and μ_2 can be solved by Eqs. (5.1) and (5.2).

effective capacitance of 6×10^{-8} F/ cm^2 divided by e (electron charge) which is extracted from Fig. 5.12 (a). The results of n_2 and n_1 are plotted versus V_g in Fig. 5.14 (a). Since now n_1 and n_2 are known, Eqs. (5.1) and (5.2) can be used to solve μ_1 and μ_2 .

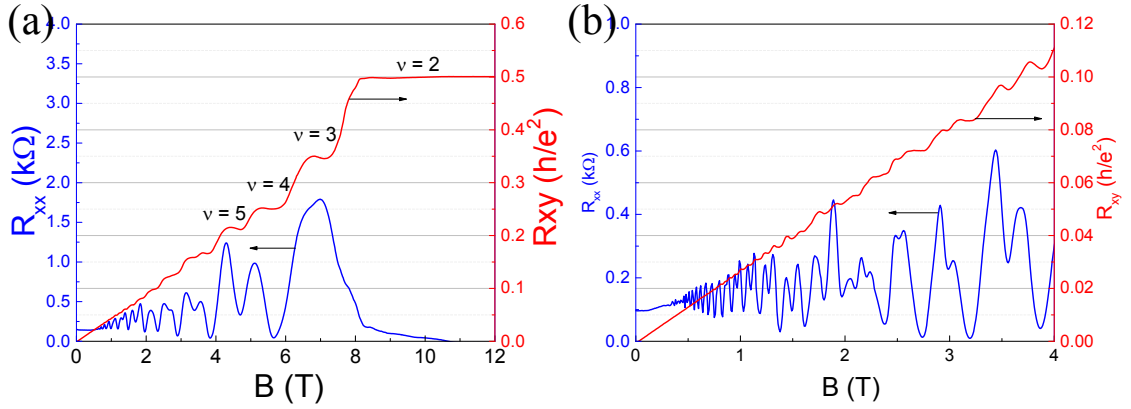


Fig. 5.15 Magneto-resistances (R_{xx} and R_{xy}) vs. magnetic field at 0.3 K of sample #5630 at (a) $V_g = 3$ V and (b) $V_g = 4$ V.

The mobilities in the first and second subbands are plotted in Fig. 5.14 (b). Both increase with V_g because of stronger screening by the increased electrons in the second subband, which follows the experimental results in [103, 105]. Note that μ_1 and μ_{Hall} are very close near the onset of the second subband occupancy, suggesting that the conduction would be dominated by the electrons in the first subband. As V_g increases, more electrons populated in the second subband, so the deviation between μ_1 and μ_{Hall} becomes larger due to the stronger participation of the second subband.

Magneto-resistances (R_{xx} and R_{xy}) vs. magnetic field at 0.3 K for sample #5630 at $V_g = 3$ V are shown in Fig. 5.15 (a). The onsets of Shubnikov-de Haas oscillations in R_{xx} and flat quantum Hall plateaus in R_{xy} occurred at 0.6 T and 0.9 T, respectively, showing the high quality of this inverted device. The spin splitting and valley splitting occurred at $B = 1.3$ T and 2.6 T. It is thought-provoking to note there is no $\nu = 3$ in R_{xx} , despite the presence of the Hall plateau in R_{xy} , which we do not understand yet. The vanishing longitudinal magneto-resistance (R_{xx}) indicates there is no parallel conduction from the bottom doped layer. Furthermore, a single period of R_{xx} vs.

(1/B) suggests only one two-dimensional channel exists. As the gate voltage increases, the presence of the beating of the oscillations in R_{xx} indicates the onset of the occupancy of the second subband (Fig. 5.15 (b)).

5.3.4 Comparison of 2DEG Mobility in Different Structures

In this thesis, we studied three different structures of Si 2DEGs: standard modulation-doped Si 2DEG (with a doping layer on top of the Si QW), an inverted modulation-doped Si 2DEG (with a doping layer on the bottom of the Si QW), and an enhancement-mode ^{28}Si enriched 2DEG without any doping layer. The relationship of μ and n at 4 K for those structures are plotted in Fig. 5.16 with the results of enhancement-mode 2DEG of natural Si also shown for comparison (courtesy of Chiao-Ti Huang). Clearly, at electron density below $3 \times 10^{11} \text{ cm}^{-2}$, the mobilities for all structures are almost identical with a slope of $\mu \propto n^{1.5}$. For those four structures, the distance from the 2DEG to the surface is 50 ~ 60 nm regardless of the presence of the doping layers except top-doped sample (#5737) with a distance of 100 nm from the surface to the 2DEG and a distance of 50 nm from the remote doped layer to the underlying 2DEG (Fig. 4.19(a)).

Based on the prior theoretical or experimental work [82, 91], if the exponent of $\mu \propto n^\alpha$ is close to 1.5, it is suggested the remote impurity scattering would be the dominant scattering mechanism. In Fig. 5.16, all curves of mobility vs. density show their exponents close to 1.5, which seems support our arguments on the limiting scattering mechanism. For quantum dot applications, a low electron density of $\sim 1 \times$

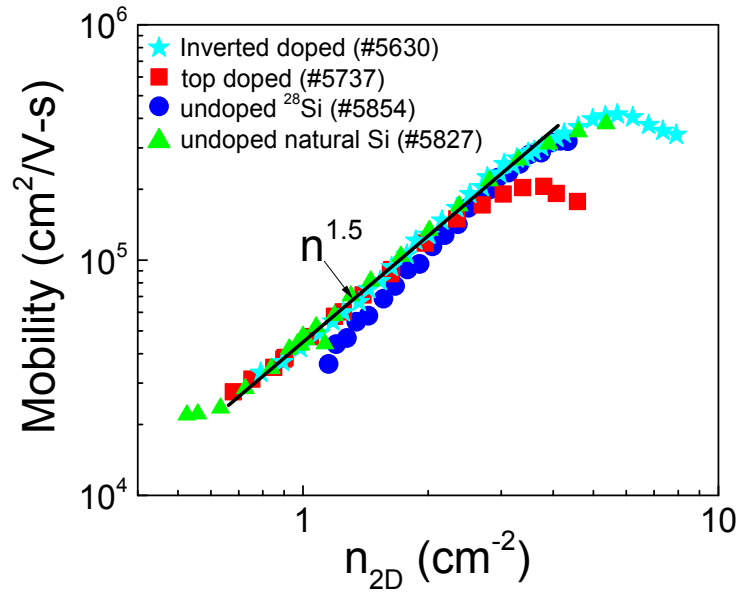


Fig. 5.16 Mobility vs. density at 4 K for different structures of Si 2DEGs in this thesis.

10^{11} cm^{-2} or below has been suggested. To enhance the electron mobility in this regime, a larger distance between the surface and the 2DEG can be used to reduce the remote scattering. However, for fine gating of 2DEG devices, a short distance is required. Thus, the improvement of the remote Si/Al₂O₃ interface without increasing the distance between the surface and the 2DEG is required. Further work on the understanding of the Si/Al₂O₃ interfacial properties is required.

5.4 Summary

We first studied isotopically enriched ²⁸Si 2DEGs, which can be used to increase the spin decoherence time for quantum computing applications. By the enrichment of ²⁸Si, the only spin-carrying isotope of ²⁹Si was reduced from 4.7 % to 800

ppm with a predicted dephasing time of 2 μ s. Furthermore, a high mobility of 522,000 $\text{cm}^2/\text{V}\cdot\text{s}$ at 0.3 K in an enriched ^{28}Si 2DEG was reported with clear Hall plateaus and Shubnikov-de Haas oscillations, showing its high material quality. By top gating, remote impurity charges at the $\text{Si}/\text{Al}_2\text{O}_3$ interface was suggested as the dominant scattering source, and an extremely low free electron density of $6 \times 10^{10} \text{ cm}^{-2}$ was also presented.

Then we present an inverted modulation-doped Si 2DEGs of high mobility $\sim 470,000 \text{ cm}^2/\text{V}\cdot\text{s}$ at 0.3 K by the suppression of phosphorus segregation in the lower SiGe setback layer. We showed that the sharp P turn-off ($< 10 \text{ nm/decade}$) is a key to the success of high-quality inverted structures. An inverted modulation-doped Si 2DEG of high mobility by reducing phosphorus segregation opens the path towards the first demonstration of a bilayer device of two adjacent Si 2DEGs. Second subband occupancy and the intersubband scattering of electron between the first and second subbands were also demonstrated for the first time in a Si 2DEG.

It is interesting to note that μ vs. n , in a enhancement-mode structure Si 2DEG of isotopically enriched ^{28}Si , in a enhancement-mode 2DEG of natural Si, in a standard modulation-doped (top-doped) Si 2DEG, and in a inverted modulation-doped (bottom-doped) Si 2DEG, all with the distance of 50 \sim 60 nm from the 2DEG layer to the remote impurity layer such as the supply layer or the Si surface layer, shows a strikingly similar form. It seems electron mobility was limited by the remote impurity scattering at the Si surface.

Chapter 6 Conclusions and Future Work

6.1 Conclusions

Strained Si and SiGe quantum devices were made from structures grown by CVD. First, we presented the work of band-to-band tunneling in strained SiGe, which is crucial for Si-based tunneling FETs for low-power applications. We investigated the effects of electric field and Ge fraction on band-to-band tunneling (BTBT) in p^+ -SiGe/ n^+ -Si heterojunctions and p^+ -SiGe/ n^+ -SiGe homojunctions at both forward and reverse biases. Negative differential resistance (NDR) was observed for each device, showing the high quality of tunneling devices by CVD. A peak current density of 8.2 kA/cm^2 in forward bias and reverse-biased BTBT current density of 10^3 kA/cm^2 at -1 V were demonstrated, both of which we believed to be the highest among all Si-based tunneling diodes by CVD. Furthermore, we also showed the importance of the presence of NDR in forward bias to distinguish between direct BTBT and defect-assisted tunneling in reverse bias. Good agreement between experimental results and models for forward and reverse biases was achieved, which can serve as a basis for the related tunneling device modeling.

Next, we studied the surface segregation of phosphorus in relaxed SiGe epitaxial layers and investigated the effects of surface hydrogen. We experimentally observed an opposite trend of phosphorus segregation versus temperature compared to that expected from the prediction of a two-state model (TSM). We proposed a phenomenological model that accounts for the effect of surface hydrogen on the

segregation energy of phosphorus. Surface hydrogen changes the bonding structure of host atoms (Si or Ge) in the surface layer and reduces the segregation energy. An extremely sharp P turn-off slope of 6 nm/dec was also achieved, enabling effective Schottky gating on modulation-doped Si two-dimensional electron gas.

Two-dimensional electron gases (2DEGs) in a strained Si are promising for quantum dot applications. We investigated the transport properties in Si 2DEGs grown in Princeton and achieved a mobility of 522,000 cm²/V-s at 0.3 K, among the best by CVD. This was attributed to the reduction of the phosphorus background level in the CVD system by a gas separation system of the doping gas of phosphorus and other process gases. The effects of different layers on ungated depletion-mode devices of modulation-doped Si 2DEG were investigated. The results showed that the remote impurity charges at the supply layer were the major source of electron scattering. The experimental results of top Schottky gated devices also supported this conclusion.

In Si of natural abundance, only the 4.7 % atoms of ²⁹Si carry nuclear spins, leading to spin decoherence. ²⁸Si enrichment reduced the level of ²⁹Si to 800 ppm, which could extend the dephasing time in QDs to 2μs, 300 times longer than that in GaAs QDs. High mobility of 522,000 cm²/V-s in an isotopically enriched ²⁸Si 2DEG was also reported. The remote impurity charges at the supply layer for the depletion-mode devices and at the Si/Al₂O₃ interface for the enhancement-mode devices were considered the main source for electron scattering.

Last, an inverted modulation-doped 2DEG with Si of natural abundance achieved a record high mobility of 470,000 cm²/V-s at 0.3 K. High mobility in this type of structure was attributed to the lower phosphorus level by strong reduction of

phosphorus segregation, which was enabled by low-temperature epitaxy. Furthermore, we experimentally presented the occupancy of the second subband and intersubband scattering between the first and second subbands in a Si 2DEG for the first time. The fact that the initial drop and subsequent rise in the measured Hall mobility because of the intersubband scattering were observed supported our conclusions.

6.2 Future Work

In this section, some aspects of considerable interest about the topics in this thesis are given as follows:

(i) Band-to-band tunneling devices:

Based on the results in chapter 2, SiGe-based BTBT is promising for the realization of TFET of high performance. However, there is no report on any Si-based TFET with a high drive current as high as $100 \mu\text{A}/\mu\text{m}$ and a sharp sub-threshold slope of $< 60 \text{ mV/decade}$ at the same time, which is crucial for the replacement of conventional MOSFETs. Further work on the comparison of the TFET experiment and modeling based on our experimental results from diode structures will be required for further development of TFETs.

(ii) Phosphorus segregation:

In chapter 2, phosphorus turn-off slopes in strained and relaxed $\text{Si}_{0.7}\text{Ge}_{0.3}$ films were different. A further analysis is required to explain this observation. Moreover, since the hydrogen coverage depends on the Ge fraction in SiGe alloys, the effect of hydrogen

on the bonding structure and segregation energy of phosphorus near the surface could also be different for various Ge fractions.

(iii) Si 2DEG:

While high mobility in Si 2DEGs was demonstrated by our CVD, the predicted upper limit of mobility is still much higher than our experimental results. Further work is required to determine the missing factor. In addition, the process of second subband occupancy is not completely understood, although some convincing evidence was presented. Last, the high-mobility inverted modulation-doped Si 2DEG enables the growth of a bilayer of parallel Si 2DEGs.

Bibliography

- [1] <http://www.statisticbrain.com/computer-sales-statistics/>
- [2] http://en.wikipedia.org/wiki/Transistor_count
- [3] Y. Taur and T. H. Ning, *Fundamentals of Modern VLSI Devices*, Cambridge, 2002.
- [4] A. M. Ionescu and H. Riel, “Tunnel field-effect transistors as energy-efficient electronic switches,” *Nature*, vol. 479, pp. 329 – 337, 2011.
- [5] T. D. Ladd, F. Jelezko, R. Laflamme, Y. Nakamura, C. Monroe, and J. L. O’Brien, “Quantum computers,” *Nature*, vol. 464, pp. 45 – 53, 2010.
- [6] T. Baba, “Proposal for surface tunnel transistors,” *Japanese Journal of Applied Physics*, vol. 31, pp. L455 – L457, 1992.
- [7] S. G. Thomas, P. Tomasini, M. Bauer, B. Vyne, Y. Zhang, M. Givens, J. Devrajan, S. Koester, and I. Lauer, “Enabling Moore’s law beyond CMOS technologies through heteroepitaxy,” *Thin Solid Films*, vol. 518, pp. S53 – S56, 2010.
- [8] P. Shor, “Polynomial-time algorithms for prime factorization and discrete logarithms on a quantum computer,” *SIAM Journal of Computing*, vol. 26, pp. 1484 – 1509, 1997.
- [9] N. A. Gershenfeld and I. L. Chuang, “Bulk spin-resonance quantum computation,” *Science*, vol. 275, pp. 350 – 356, 1997.
- [10] L. B. Ioffe, V. B. Geshkenbein, M. V. Feigel’man, A. L. Fauchère, and G. Blatter, “Environmentally decoupled *sds*-wave Josephson junctions for quantum computing,” *Nature*, vol. 398, pp. 679 – 681, 1999.
- [11] A. C. Johnson, J. R. Petta, J. M. Taylor, A. Yacoby, M. D. Lukin, C. M. Marcus, M. P. Hanson, and A. C. Gossard, “Triplet-singlet spin relaxation via nuclei in a double quantum dot,” *Nature*, vol. 435, pp. 925 – 928, 2005.
- [12] J. R. Petta, A. C. Johnson, J. M. Taylor, E. A. Laird, A. Yacoby, M. D. Lukin, C. M. Marcus, M. P. Hanson, and A. C. Gossard, “Coherent manipulation of coupled electron spins in semiconductor quantum dots,” *Science*, vol. 309, pp.

2180 – 2184, 2005.

- [13] B. M. Maune, M. G. Borselli, B. Huang, T. D. Ladd, P. W. Deelman, K. S. Holabird, A. A. Kiselev, I. Alvarado-Rodriguez, R. S. Ross, A. E. Schmitz, M. Sokolich, C. A. Watson, M. F. Gyure, and A. T. Hunter, “Coherent singlet-triplet oscillations in a silicon-based double quantum dot,” *Science*, vol. 481, pp. 344 – 347, 2012.
- [14] L. Esaki, “New phenomenon in narrow germanium p-n junctions,” *Physical Review*, vol. 109, pp. 603 – 604, 1958.
- [15] P. See, D. J. Paul, B. Holländer, S. Mantl, I. V. Zozoulenko, and K. -F. Berggren, “High performance Si/Si_{1-x}Ge_x resonant tunneling diodes,” *IEEE Electron Device Letters*, vol. 22, pp. 182 – 184, 2001.
- [16] J. Faist, F. Capasso, D. H. L. Sivco, C. Sirtori, A. L. Hutchinson, A. Y. Cho, “Quantum cascade laser,” *Science*, vol. 264, pp. 553 – 556, 1994.
- [17] A. C. Seabaugh and Q. Zhang, “Low-voltage tunnel transistors for beyond CMOS logic,” *Proceedings of IEEE*, vol. 98, pp. 2095 – 2110, 2010.
- [18] W. Y. Choi, B. -G. Park, J. D. Lee, and T. -J. K. Liu, “Tunneling field-effect transistors (TFETs) with subthreshold swing (SS) less than 60 mV/dec,” *IEEE Electron Device Letters*, vol. 28, pp. 743 – 745, 2007.
- [19] E. Kasper and K. Lyutovich, *Properties of Silicon Germanium and SiGe:Carbon*, INSPEC, 2000.
- [20] K. K. Bhuiwarka, J. Schulze, I. Eisele, “Performance enhancement of vertical tunnel field-effect transistor with SiGe in the δp^+ layer,” *Japanese Journal of Applied Physics*, vol. 43, pp. 4073 – 4078, 2004.
- [21] M. Schmidt, R. A. Minamisawa, S. Richter, R. Luptak, J. -M. Hartmann, D. Buca, Q. T. Zhao, and S. Mantl, “Impact of strain and Ge concentration on the performance of planar SiGe band-to-band-tunneling transistors,” *Solid-State Electronics*, vol. 71, pp. 42 – 47, 2012.
- [22] L. Esaki, “Discovery of the tunnel diode,” *IEEE Transactions on Electron Devices*, vol. 23, pp. 644 – 647, 1976.
- [23] http://www3.nd.edu/~gsnider/1D_Poi_PC_b8j.zip
- [24] S. M. Sze and K. K. Ng, *Physics of Semiconductor Devices*, Wiley, 2006.

- [25] E.O. Kane, "Theory of tunneling," *Journal of Applied Physics*, vol. 32, pp. 83 – 91, 1961.
- [26] A. G. Chynoweth, W. L. Feldmann, and R. A. Logan, "Excess tunnel current in silicon Esaki junctions," *Physical Review*, vol. 121, pp. 684 – 694, 1961.
- [27] C. T. Sah, "Electronic processes and excess currents in gold-doped narrow silicon junctions," *Physical Review*, vol. 123, pp. 1594 – 1612, 1961.
- [28] B. D. Weaver, P. E. Thompson, N. Jin, S. -Y. Chung, A. T. Rice, and P. R. Berger, "Radiation tolerance of Si/Si_{0.6}Ge_{0.4} resonant interband tunneling diodes," *Journal of Applied Physics*, vol. 95, no. 11, pp. 6406 – 6408, 2004.
- [29] M. Yang, *Sub-100 nm Vertical MOSFET's with Si_{1-x-y}Ge_xC_y Source/Drains*, Ph.D. dissertation, Princeton University, 2000.
- [30] G. Gillen, R. Lareau, J. Bennett, and F. Stevie, *Secondary Ion Mass Spectrometry*, Wiley, 1998.
- [31] J. E. Greene, S. A. Barnett, A. Rockett, and G. Bajor, "Modeling of dopant incorporation, segregation, and ion/surface interaction effects during semiconductor film growth by molecular beam epitaxy and plasma-based techniques," *Applications of Surface Science*, vol. 22/23, pp. 520 – 544, 1985.
- [32] M. Bao and K. L. Wang, "Accurately measuring current-voltage characteristics of tunnel diodes," *IEEE Transactions on Electron Devices*, vol. 53, pp. 2564 – 2568, 2006.
- [33] R. People and J. C. Bean, "Calculation of critical layer thickness versus lattice mismatch for Ge_xSi_{1-x}/Si strained-layer heterostructures," *Applied Physics Letters*, vol. 47, pp. 322 – 324, 1985.
- [34] D. J. Robbins, L. T. Canham, S. J. Barnett, A. D. Pitt, and P. Calcott, "Near-band-gap photoluminescence from pseudomorphic Si_{1-x}Ge_x single layers on silicon," *Journal of Applied Physics*, vol. 71, pp. 1407 – 1414, 1992.
- [35] R. Braunstein, A. R. Moore, and F. Herman, "Intrinsic optical absorption in germanium-silicon alloys," *Physical Review*, vol. 109, pp. 695 – 710, 1958.
- [36] R. B. Fair and H. W. Wivell, "Zener and avalanche breakdown in As-implanted low-voltage Si n-p junctions," *IEEE Transactions on Electron Devices*, vol. 23, pp. 512 – 518, 1976.

- [37] J. M. C. Stork and R. D. Isaac, "Tunneling in base-emitter junctions," *IEEE Transactions on Electron Devices*, vol. 30, pp. 1527 – 1534, 1983.
- [38] X. Guo and E. F. Schubert, "Current crowding and optical saturation effects in GaInN/GaN light-emitting diodes grown on insulating substrates," *Applied Physics Letters*, vol. 78, pp. 3337 – 3339, 2001.
- [39] P. Fay, J. Lu, Y. Xu, G. H. Bernstein, D. H. Chow, and J. N. Schulman, "Microwave performance and modeling of InAs/AlSb/GaSb resonant interband tunneling diodes," *IEEE Transaction on Electron Devices*, vol. 49, pp. 19 – 24, 2002.
- [40] A. Ramesh, T. A. Growden, P. R. Berger, R. Loo, W. Vandervorst, B. Douhard, and M. Caymax, "Boron delta-doping dependence on Si/SiGe resonant interband tunneling diodes grown by chemical vapor deposition," *IEEE Transactions on Electron Devices*, vol. 59, pp. 602 – 609, 2012.
- [41] C. Payette, K. Wang, P. J. Koppinen, Y. Dovzhenko, J. C. Sturm, and J. R. Petta, "Single charge sensing and transport in double quantum dots fabricated from commercially grown Si/SiGe heterostructures," *Applied Physics Letters*, vol. 100, p. 043508, 2012.
- [42] D. V. Yurasov, M. N. Drozdov, A. V. Murel, M. V. Shaleev, N. D. Zakharov, and A. V. Novikov, "Usage of antimony segregation for selective doping of Si in molecular beam epitaxy," *Journal of Applied Physics*, vol. 109, p. 113533, 2011.
- [43] K. D. Hobart, F. J. Kub, G. G. Jernigan, and P. E. Thompson, "Surface segregation of arsenic and phosphorus from buried layers during Si molecular beam epitaxy," *Journal of Vacuum Science and Technology B*, vol. 14, pp. 2229 – 2232, 1996.
- [44] M. Yang, M. Carroll, J. C. Sturm, and T. Büyüklımanlı, "Phosphorus doping and sharp profiles in silicon and silicon-germanium epitaxy by rapid thermal chemical vapor deposition," *Journal of the Electrochemical Society*, vol. 147, pp. 3541 – 3545, 2000.
- [45] D. V. Singh, J. L. Hoyt, and J. F. Gibbons, "Abrupt phosphorus profiles in Si: Effects of temperature and substitutional carbon on phosphorus autodoping,"

- Journal of Electrochemical Society*, vol. 150, pp. G553 – G556, 2003.
- [46] J. Tersoff, “Carbon defects and defect reactions in silicon,” *Physical Review Letters*, vol. 64, pp. 1757 – 1760, 1990.
- [47] J. F. Nützel and G. Abstreiter, “Comparison of P and Sb as n-dopants for Si molecular beam epitaxy,” *Journal of Applied Physics*, vol. 78, pp. 937 – 940, 1995.
- [48] J. J. Harris, D. E. Ashenford, C. T. Foxon, P. J. Dobson, and B. A. Joyce, “Kinetic limitations to surface segregation during MBE growth of III-V compounds: Sn in GaAs,” *Applied Physics A*, vol. 33, pp. 87 – 92, 1984.
- [49] B. Cho, J. Bareño, Y. L. Foo, S. Hong, T. Spila, I. Petrov, and J. E. Greene, “Phosphorus incorporation during Si (001):P gas-source molecular beam epitaxy: Effects on growth kinetics and surface morphology,” *Journal of Applied Physics*, vol. 103, p. 123530, 2008.
- [50] M. L. Yu, D. J. Vitkavage, and B. S. Meyerson, “Doping reaction of PH₃ and B₂H₆ with Si(100),” *Journal of Applied Physics*, vol. 59, pp. 4032 – 4037, 1986.
- [51] P. Sen, B. C. Gupta, and I. P. Batra, “Structures studies of phosphorus induced dimers on Si(001),” *Physical Review B*, vol. 73, p. 085319, 2006.
- [52] J. F. Nützel, M. Holzmann, P. Schittenhelm, and G. Abstreiter, “Segregation of n-dopants on SiGe surfaces,” *Applied Surface Science*, vol. 102, pp. 98 – 101, 1996.
- [53] M. -H. Xie, A. K. Lees, J. M. Fernandez, J. Zhang, and B. A. Joyce, “Arsenic surface segregation and incorporation in Si and Si_{1-x}Ge_x during gas source molecular beam epitaxy,” *Journal of Crystal Growth*, vol. 173, pp. 336 – 342, 1997.
- [54] M. -H. Xie, J. Zhang, A. Lees, J. M. Fernandez, and B. A. Joyce, “Surface segregation during molecular beam epitaxy: the site-blocking effects of surfactant atoms,” *Surface Science*, vol. 367, pp. 231 – 237, 1996.
- [55] H. Kim, N. Taylor, J. R. Abelson, and J. E. Greene, “Effects of H coverage on Ge segregation during Si_{1-x}Ge_x gas-source molecular beam epitaxy,” *Journal of Applied Physics*, vol. 82, pp. 6062 – 6066, 1997.

- [56] J. Y. Li, C. T. Huang, J. C. Sturm, "The effect of hydrogen on the surface segregation of phosphorus in epitaxially grown relaxed $\text{Si}_{0.7}\text{Ge}_{0.3}$ films by rapid thermal chemical vapor deposition," *Applied Physics Letters*, vol. 101, p. 142112, 2012.
- [57] L. Oberbeck, N. J. Curson, T. Hallam, M. Y. Simmons, G. Bilger, and R. G. Clark, "Measurement of phosphorus segregation in silicon at the atomic scale using scanning tunneling microscopy," *Applied Physics Letters*, vol. 85, pp. 1359 – 1361, 2004.
- [58] J. F. Nützel and G. Abstreiter, "Segregation and diffusion on semiconductor surfaces," *Physical Review B*, vol. 53, pp. 13551 – 13558, 1996.
- [59] E. S. Tok, S. W. Ong, and H. Chuan Kang, "Hydrogen desorption kinetics from the $\text{Si}_{1-x}\text{Ge}_x(100)-(2\times 1)$ surface," *Journal of Chemical Physics*, vol. 120, pp. 5424 – 5431, 2004.
- [60] M. P. D'Evelyn, S. M. Cohen, E. Rouchouze, and Y. L. Yang, "Surface π bonding and the near-first-order desorption kinetics of hydrogen from $\text{Ge}(100)2\times 1$," *Journal of Chemical Physics*, vol. 98, pp. 3560 – 3563, 1993.
- [61] D. A. Grützmacher, T. O. Sedgwick, A. Powell, M. Tejwani, S. S. Iyer, J. Cotte, and F. Cardone, "Ge segregation in SiGe/Si heterostructures and its dependence on deposition technique and growth atmosphere," *Applied Physics Letters*, vol. 63, pp. 2531 – 2533, 1993.
- [62] M. J. -P. Duchemin, M. M. Bonnet, and M. F. Koelsch, "Kinetics of silicon growth under low hydrogen pressure," *Journal of the Electrochemical Society*, vol. 125, pp. 637 – 644, 1978.
- [63] T. Ando, A. B. Fowler, and F. Stern, "Electronic properties of two-dimensional system," *Review of Modern Physics*, vol. 54, pp. 437 – 672, 1982.
- [64] K. Klitzing, G. Dorda, and M. Pepper, "New method for high-accuracy determination of the fine-Structure constant based on quantized Hall resistance," *Physical Review Letters*, vol. 45, pp. 494 – 497, 1980.
- [65] D. C. Tsui, H. L. Störmer, A. C. Gossard, "Two-dimensional magnetotransport in the extreme quantum limit," *Physical Review Letters*, vol. 48, pp. 1559 – 1562, 1982.

- [66] K. Ismail, J. O. Chu, and M. Arafa, "Integrated enhancement- and depletion-mode FET's in modulation-doped Si/SiGe heterostructures," *IEEE Electron Device Letters*, vol. 18, pp. 435 – 437, 1997.
- [67] R. Dingle, H. L. Störmer, A. C. Gossard, "Electron mobilities in modulation-doped semiconductor heterojunctions superlattices," *Applied Physics Letters*, vol. 33, pp. 665 – 667, 1978.
- [68] V. Umansky, M. Heiblum, Y. Levinson, J. Smet, J. Nübler, and M. Dolev, "MBE growth of ultra-low disorder 2DEG with mobility exceeding 35×10^6 cm²/Vs," *Journal of Crystal Growth*, vol. 311, pp. 1658 – 1661, 2009.
- [69] M. Xiao, M. G. House, and H. W. Jiang, "Measurement of the spin relaxation time of single electrons in a silicon metal-oxide-semiconductor-based quantum dot," *Physical Review Letters*, vol. 104, p. 096801, 2010.
- [70] G. Abstreiter, H. Brugger, T. Wolf, H. Jorke, and H. J. Herzog, "Strained-induced two-dimensional electron gas in selectively doped Si/Si_xGe_{1-x} superlattices," *Physical Review Letters*, vol. 54, pp. 2441 – 2444, 1985.
- [71] K. Ismail, M. Arafa, K. L. Saenger, J. O. Chu, and B. S. Meyerson, "Extremely high electron mobility in Si/SiGe modulation-doped heterostructures," *Applied Physics Letters*, vol. 66, pp. 1077 – 1079, 1995.
- [72] N. Sugii, K. Nakagawa, Y. Kimura, S. Yamaguchi, and M. Miyao, "High electron mobility in strained Si channel of Si_{1-x}Ge_x/Si/Si_{1-x}Ge_x heterostructure with abrupt interface," *Semiconductor Science and Technology*, vol. 13, pp. A140 – A142, 1998.
- [73] S. -H. Huang, T. -M. Lu, S. -C. Lu, C. -H. Lee, C. W. Liu, and D. C. Tsui, "Mobility enhancement of strained Si by optimized SiGe/Si/SiGe structures," *Applied Physics Letters*, vol. 101, p. 042111, 2012.
- [74] M. Kim and H. J. Osten, "X-ray photoelectron spectroscopy evaluation of valence band offsets for strained Si_{1-x}Ge_x, Si_{1-y}C_y, and Si_{1-x-y}Ge_xC_y on Si(001)," *Applied Physics Letters*, vol. 70, pp. 2702 – 2704, 1997.
- [75] D. J. Paul, "Si/SiGe heterostructures: from material and physics to devices and circuits," *Semiconductor Science and Technology*, vol. 19, pp. R75 – R108,

- 2004.
- [76] G. P. Watson, E. A. Fitzgerald, Y. -H. Xie, and D. Monroe, “Relaxed low threading defect density Si_{0.7}Ge_{0.3} epitaxial layers grown on Si by rapid thermal chemical vapor deposition,” *Journal of Applied Physics*, vol. 75, pp. 263 – 269, 1994.
- [77] Y. Sun, Z. Liu, S. Sun, and P. Pianetta, “The effectiveness of HCl and HF cleaning of Si_{0.85}Ge_{0.15} surface,” *Journal of Vacuum Science and Technology A*, vol. 26, pp. 1248 – 1250, 2008.
- [78] D. J. Paul, A. Ahmed, M. Pepper, A. C. Churchill, D. J. Robbins, D. J. Wallis, and A. J. Pidduck, “Electrical properties and uniformity of two dimensional electron gases grown on cleaned SiGe virtual substrates,” *Journal of Vacuum Science and Technology B*, vol. 16, pp. 1644 – 1647, 1998.
- [79] J. H. Davies, *The Physics of Low-Dimensional Semiconductors*, Cambridge, 1998.
- [80] R. People and J. C. Bean, “Band alignments of coherently strained Ge_xSi_{1-x}/Si heterostructures on <001> Ge_ySi_{1-y} substrates,” *Applied Physics Letters*, vol. 48, pp. 538 – 540, 1986.
- [81] A. Gold, “Electronic transport properties of a two-dimensional electron gas in a silicon quantum-well structure at low temperature,” *Physical Review B*, vol. 35, pp. 723 – 733, 1987.
- [82] D. Monroe, Y. -H. Xie, E. A. Fitzgerald, P. J. Silverman, and G. P. Watson, “Comparison of mobility-limiting mechanisms in high-mobility Si_{1-x}Ge_x heterostructures,” *Journal of Vacuum Science and Technology B*, vol. 11, pp. 1731 – 1737, 1993.
- [83] G. I. Ritter, B. Tillack, and D. Wolansky, “Memory effect in RTCVD epitaxy of Si and SiGe,” *MRS Proceedings*, vol. 429, pp. 379 – 384, 1996.
- [84] J. Y. Li, C. T. Huang, L. P. Rokhinson, and J. C. Sturm, “Extremely low electron density in a modulation-doped Si/SiGe two-dimensional electron gases by effective Schottky gating,” *ECS Transactions*, vol. 50, pp. 145 – 149, 2012.
- [85] C. A. Richter, R. G. Wheele, and R. N. Sacks, “Overshoots of quantum Hall plateaus,” *Surface Science*, vol. 263, pp. 270 – 274, 1992.

- [86] S. Komiyama, H. Nii, M. Ohsaw, S. Fukatsu, Y. Shiraki, R. Itoh, and H. Toyoshima, "Resistance and resistivity of two dimensional electron gas at high magnetic fields," *Solid State Communications*, vol. 80, pp. 157 – 163, 1991.
- [87] J. W. Matthews and A. E. Blakeslee, "Defects in epitaxial multilayers: I. Misfit dislocations," *Journal of Crystal Growth*, vol. 27, pp. 118 – 125, 1974.
- [88] H. Sakaki, T. Noda, K. Hirakawa, M. Tanaka, and T. Matsusue, "Interface roughness scattering in GaAs/AlAs quantum wells," *Applied Physics Letters*, vol. 51, pp. 1934 – 1936, 1987.
- [89] A. Gold, "Mobility and metal–insulator transition of the two-dimensional electron gas in SiGe/Si/SiGe quantum wells," *Journal of Applied Physics*, vol. 108, p. 063710, 2010.
- [90] J. A. Nixon and J. H. Davies, "Potential fluctuations in heterostructure devices," *Physical Review B*, vol. 41, pp. 7929 – 7932, 1990.
- [91] D. Laroche, S. Das Sarma, G. Gervais, M. P. Lilly, and J. L. Reno, "Scattering mechanism in modulated-doped shallow two-dimensional electron gas," *Applied Physics Letters*, vol. 96, p. 162112, 2010.
- [92] Z. Wilamowski, N. Sandersfeld, W. Jantsch, D. Többen, and F. Schäffler, "Screening breakdown on the route toward the metal-insulator transition in modulation-doped Si/SiGe quantum wells," *Physical Review Letters*, vol. 87, p. 026401, 2001.
- [93] E. F. Schubert, K. Ploog, H. Dämbkes, and K. Heime, "Selectively doped n-Al_xGa_{1-x}As/GaAs heterostructures with high-mobility two-dimensional electron gas for field effect transistors," *Applied Physics A*, vol. 33, pp. 63 – 76, 1984.
- [94] M. A. Reed, W. P. Kirk, and P. S. Kobiela, "Investigating of parallel conduction in GaAs/Al_xGa_{1-x}As modulation-doped structures in the quantum limit," *IEEE Journal of Quantum Electronics*, vol. 22, pp. 1753 – 1759, 1986.
- [95] K. Ensslin, D. Heitmann, R. R. Gerhardts, and K. Ploog, "Population process of the upper subband in Al_xGa_{1-x}As-GaAs quantum wells," *Physical Review B*, vol. 39, pp. 12993 – 12996, 1989.
- [96] T. M. Lu, C. -H. Lee, S. -H. Huang, D. C. Tsui, and C. W. Liu, "Upper limit of two-dimensional electron density in enhancement-mode Si/SiGe

- heterostructure field-effect transistors,” *Applied Physics Letters*, vol. 99, p. 153510, 2011.
- [97] D. R. Lide, *CRC Handbook of Chemistry and Physics*, CRC Press, 2006.
- [98] A. Wild, J. Kierig, J. Sailer, J. W. Ager III, E. E. Haller, G. Abstreiter, S. Ludwig, and D. Bougeard, “Few electron double quantum dot in an isotopically purified ^{28}Si quantum well,” *Applied Physics Letters*, vol. 100, p. 143110, 2012.
- [99] L. V. C. Assali, H. M. Petrilli, R. B. Capaz, B. Koiller, X. Hu, and S. Das Sarma, “Hyperfine interactions in silicon quantum dots,” *Physical Review B*, vol. 83, p. 165301, 2011.
- [100] K. Yao, *Silicon and Silicon-Germanium Epitaxy for Quantum Dot Device Fabrications towards an Electron Spin-Based Quantum Computer*, Ph.D. dissertation, Princeton University, 2009.
- [101] M. Kellogg, J. P. Eisenstein, L. N. Pfeiffer, and K. W. West, “Vanishing Hall resistance at high magnetic field in a double-layer two-dimensional electron system,” *Physical Review Letters*, vol. 93, p. 036801, 2004.
- [102] D.J. Paul, A. Ahmed, A.C. Churchill, D.J. Robbins, and W.Y. Leong, “Low-dimensional inverted Si/SiGe modulation-doped electron gases using selective ex-situ ion implantation,” *Materials Science and Engineering B*, vol. 89, pp. 111 – 115, 2002.
- [103] H. L. Störmer, A. C. Gossard, and W. Wiegmann, “Observation of intersubband scattering in a 2-dimensional electron system,” *Solid State Communications*, vol. 41, pp. 707 – 709, 1982.
- [104] T. P. Smith III and F. F. Fang, “Upper-subband transport in GaAs heterostructures,” *Physical Review B*, vol. 37, pp. 4303 – 4305, 1988.
- [105] R. Fletcher, E. Zaremba, M. D’Iorio, C. T. Foxon, and J. J. Harris, “Evidence of a mobility edge in the second subband of an $\text{Al}_{0.33}\text{Ga}_{0.67}\text{As}$ -GaAs heterojunctions,” *Physical Review B*, vol. 38, pp. 7866 – 7869, 1988.
- [106] C. Jiang, D. C. Tsui, and G. Weimann, “Threshold transport of high-mobility two-dimensional electron gas in GaAs/AlGaAs heterostructures,” *Applied Physics Letters*, vol. 53, pp. 1533 – 1535, 1988.

Appendix: Publications and Conference

Presentations Resulting from this Thesis

Journal Articles

- [1] **Jiun-Yun Li**, C. T. Huang, L. P. Rokhinson, and J. C. Sturm, “Extremely high electron mobility in an inverted modulation-doped Si two-dimensional electron gas by a sharp turn-off of phosphorus,” manuscript in preparation.
- [2] **Jiun-Yun Li**, C. T. Huang, L. P. Rokhinson, and J. C. Sturm, “Extremely high electron mobility in isotopically enriched ^{28}Si quantum wells grown by chemical vapor deposition,” manuscript to be submitted to *Applied Physics Letters*.
- [3] **Jiun-Yun Li** and J. C. Sturm, “The effects of germanium fraction on high-field band-to-band tunneling in $\text{p}^+\text{-SiGe/n}^+\text{-SiGe}$ junctions in forward and reverse biases,” accepted for publication in *IEEE Transactions on Electron Devices*.
- [4] C. T. Huang, **Jiun-Yun Li**, and J. C. Sturm, “Implant isolation of silicon two-dimensional electron gases at 4.2 K,” *IEEE Electron Device Letters*, vol. 34, pp. 21 – 23, 2013.
- [5] **Jiun-Yun Li**, C. T. Huang, L. P. Rokhinson, and J. C. Sturm, “Extremely low electron density in a modulation-doped Si/SiGe two-dimensional electron gas by effective Schottky gating,” *ECS Transactions*, vol. 50, pp. 145 – 149, 2012.
- [6] **Jiun-Yun Li**, C. T. Huang, J. C. Sturm, ”The effect of hydrogen on the surface segregation of phosphorus in epitaxially grown relaxed $\text{Si}_{0.7}\text{Ge}_{0.3}$ films by rapid thermal chemical vapor deposition,” *Applied Physics Letters*, vol. 101, p. 142112, 2012.

Conference Presentations

- [1] C. T. Huang, ***Jiun-Yun Li***, and J. C. Sturm, “Very low electron density in undoped enhancement-mode Si/SiGe two-dimensional electron gases with thin SiGe cap layers,” *223rd Meeting of the Electrochemical Society*, Toronto, ON, Canada, May. 12 – 17, 2013.
- [2] ***Jiun-Yun Li***, C. T. Huang, L. P. Rokhinson, and J. C. Sturm, “Extremely low electron density in a modulation-doped Si/SiGe 2DEG by effective Schottky gating,” *222nd Meeting of the Electrochemical Society*, Honolulu, HI, Oct. 7 – 12, 2012.
- [3] ***Jiun-Yun Li***, C. T. Huang, and J. C. Sturm, “Extremely sharp phosphorus turn-off slope and effect of hydrogen on phosphorus surface segregation in epitaxially-grown relaxed Si_{0.7}Ge_{0.3} by RTCVD,” *International SiGe Technology and Device Meeting*, Berkeley, CA, June 4 – 6, 2012.
- [4] C. T. Huang, ***Jiun-Yun Li***, and J. C. Sturm, “High breakdown voltage Schottky gating of doped Si/SiGe 2DEG system enabled by suppression of phosphorus surface segregation,” *International SiGe Technology and Device Meeting*, Berkeley, CA, June 4 – 6, 2012.
- [5] ***Jiun-Yun Li***, C. T. Huang, L. Rokhinson, J. A. Ohlhausen, M. S. Carroll, and J. C. Sturm, “High quality two-dimensional electron gases (2DEGs) in isotopically-enriched strained Si,” *2012 APS March Meeting Session X29*, Boston, MA, Feb. 27 – Mar. 2, 2012.
- [6] ***Jiun-Yun Li***, K. S. Chou, C. T. Huang, J. C. Sturm, and L. P. Rokhinson, “High quality two-dimensional electron gases (2DEGs) in modulation-doped and enhancement-mode Si/SiGe heterostructures,” *2011 PCCM Symposium: Quantum Control of Solid State Systems*, Princeton, NJ, Nov. 3 – 5, 2011.
- [7] ***Jiun-Yun Li***, C. T. Huang, J. C. Sturm, and L. P. Rokhinson, “High quality two-dimensional electron system (2DES) in n-Type Si/SiGe modulation-doped heterostructures grown by RTCVD,” *2011 International Workshop on Silicon Quantum Electronics*, Denver, CO, August 14 ~ 15, 2011.

- [8] K. Chou, ***Jiun-Yun Li***, C. T. Huang, J. C. Sturm, and C. W. Liu, “Stable high quality accumulation-mode Si 2DEG with a shallow top SiGe barrier of ~ 25nm,” *2011 International Workshop on Silicon Quantum Electronics*, Denver, CO, August 14 ~ 15, 2011.
- [9] ***Jiun-Yun Li***, J. C. Sturm, I. Lauer, and S. Koester, “Effect of interface defects and record high peak tunnel current density in Si-based tunnel diodes grown by RTCVD,” *2011 MRS Spring Meeting, Symposium P7.11*, San Francisco, CA, April 25 – 29, 2011.
- [10] ***Jiun-Yun Li***, J. C. Sturm, A. Majumdar, I. Lauer, and S. Koester, “Bandgap dependence of band-to-band tunneling and defect-mediated excess currents in SiGe/Si heterojunction tunnel diodes grown by RTCVD,” *67th Annual Device Research Conference (DRC 2009) Digest*, pp. 99 – 100, University Park, PA, June 22 ~ 24, 2009.